

## **Anonymous Referee #1**

Received and published: 21 April 2020

### *Comment*

*The manuscript describes the hygroscopic properties of 15 black carbon (BC) from different carbon sources using gravimetric method and DRIFTS. The authors found different BC had different mechanisms and controlling factors for equilibrium and kinetic water uptake, which mainly depended on humidity conditions. The 15 BC were characterized by many kinds of methods. The contents and constituents of OC and minerals/salts have great impact on the hygroscopic properties by this study. Therefore, it is recommended to publish on ACP after revision. Some and more detailed comments are included below:*

### Reply

We appreciate the reviewer's positive comments on the paper.

### *Comment*

*1. In the experimental part, the author should give more information of BC sources.*

### Reply

The geographic locations for collecting the biomass used in preparation of herb and woody BCPs were given in the revised paper.

More information on the two diesel soots and the household soot were also given (shown as below).

A total of 15 BCPs were tested, including 10 herb-derived BCPs, 2 wood-derived BCPs, and 3 soot-type BCPs. The herbs used for preparation of herbal BCPs were amaranth, peanuts, pea, grass, rice, wheat, corn, millet, sorghum (Nantong, Jiangsu Province, China), and bamboo (Lishui, Zhejiang Province, China), and the woods used for preparation of woody BCPs were red pine and poplar (Lishui, Zhejiang Province, China). The dried and dehydrated biomass was pulverized into a fine powder using a high-speed pulverizer (FW 100, Tianjin Taisite Instrument, China), and pyrolyzed in a muffle furnace under an oxygen-limited conditions. The oven temperature was programmed to increase from 20 to 400 °C in 2 h and maintained at 400 °C for 3 h. The Weifu diesel soot was purchased from Wuxi Weifu Automotive Diesel System Co., Ltd. (Jiangsu Province, China). According to the information provided by the manufacturer, the soot was produced under laboratory conditions by burning diesel (type # 5, China) at 1000 °C and was collected by a diesel particulate filter (NGK-6000YE) from the exhaust stream at a carbon deposition temperature of 250 °C. The diesel engine soot was collected in outdoor conditions from the freshly discharged exhaust particles on the tailpipe of a diesel truck (Dongfeng, CY4100, 2015, China) equipped with a diesel engine (CY4100Q, 3.7 L, Diesel # 0) and a diesel particulate filter (BST-5L-QCD). The household soot was collected on the inner wall

of a stove chamber (Linkou County, Heilongjiang Province, China) 1 hour later after burning of coal and wood for winter cooking and heating under limited oxygen exposure. (Page 6, lines 116-136)

*Comment*

2. *The particles should not pass through 100-mesh sieve (0.15 mm) only once, what is the particle size of the prepared BC particles? Different specific surface areas with different particle sizes will greatly affect the experimental results.*

Reply

Grounding and sieving are often applied as a standard protocol to obtain fine BCPs particles with relatively homogeneous sizes for experimental reproducibility. Please note the pretreatment would not change the compositional and structural properties of the tested BCPs.

*Comment*

3. *Lines 212-214: Why choose 30 minutes as the equilibrium time? Has the author conducted a series of equilibrium time gradient experiments to choose the preparing time?*

Reply

We understand the reviewer's concern. We measured the adsorption kinetics (see below) and found that 30 minutes were long enough to reach adsorption equilibrium. Please refer to the kinetic data below.

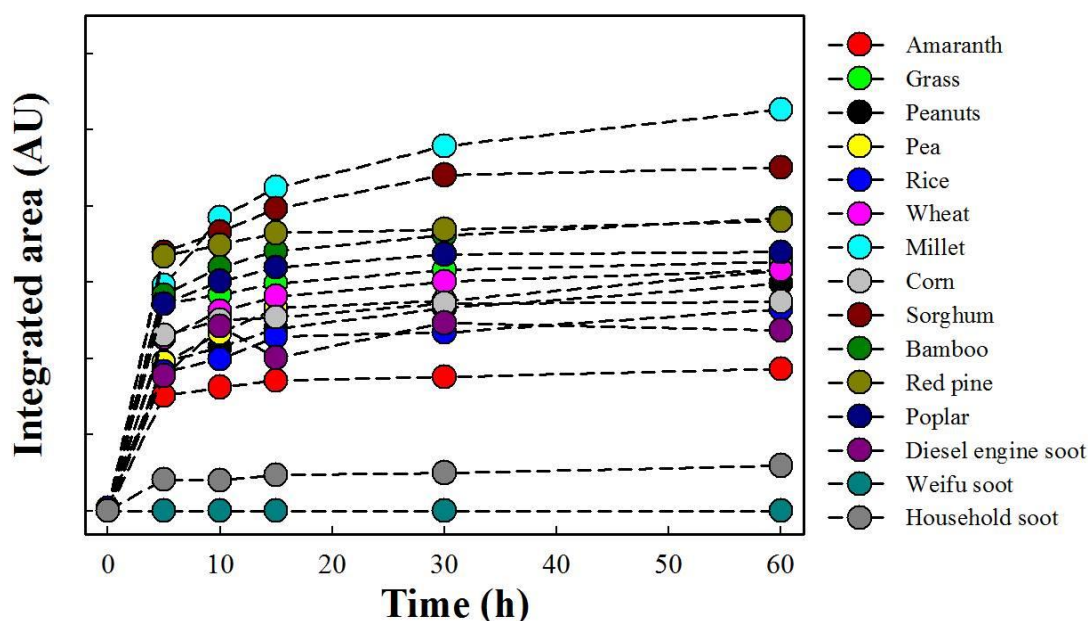


Figure R1. Equilibrium water uptake by different BCPs at 94% relative humidity measured as integrated area of O-H stretching region ( $2750\text{--}3660\text{ cm}^{-1}$ ) vs. time (h).

*Comment*

4. Line 276: the “Si” should be changed to “Si-”.

Reply

Revised. Thanks.

*Comment*

5. Line 313: The data in Figure 1 must be not done only once experiment, the error bar should be added.

Reply

Figure 1 presents sorption and desorption isotherms of water vapor to different BCPs. It is common to see that desorption isotherms of water vapor to porous media are conducted with single-point (not in replicate). With the exception of the data presented in Figure 1, all other sorption isotherm experiments were conducted in duplicate, including those for linear regression analysis. Revisions on the captions of Figures 1, 3, and 4 were made to clarify whether the data were collected in duplicate or not. The data of equilibrium water uptake for linear regression were obtained by saturated aqueous salt solutions and collected in duplicate (Figure S5). The error bars for most of the data points are smaller than the symbols.

*Comment*

6. Lines 361-363: Expect the water-soluble salts, even the insoluble compound (such as H<sub>2</sub>C<sub>2</sub>O<sub>4</sub>) could become water-soluble compound. The author can explain the phenomenon in this way.

Reply

Thanks for the suggestion. The insoluble compounds are indeed CaC<sub>2</sub>O<sub>4</sub> and/or H<sub>2</sub>C<sub>2</sub>O<sub>4</sub>. Please refer to the follow revision.

On the other hand, the poor correlation observed for C<sub>2</sub>O<sub>4</sub><sup>2-</sup> was likely due to the formation of less water-soluble compounds (e.g., CaC<sub>2</sub>O<sub>4</sub> and H<sub>2</sub>C<sub>2</sub>O<sub>4</sub>) that might depress the hygroscopicity (Buchholz and Mentel, 2008). (Page 19, lines 389-391)

*Comment*

7. Line 411: The absorption peaks of water were not unchanged, so the authors can refer to the spectra and previous study to ensure the position of those peaks. In figure 3, the signed peaks around 3600 cm<sup>-1</sup> are different from the strong peaks.

Reply

Thanks for the suggestion. Please note the wavelength of 3600 cm<sup>-1</sup> was a clerical error. It should be 3660 cm<sup>-1</sup>. The water uptake was monitored by the integrated intensity of the O-H stretching region from 2750 to 3660 cm<sup>-1</sup> according to previous study.

*Comment*

8. *Line 411: In figure 3(a), 1000 in the abscissa is shown as 100 due to layout style.*

**Reply**

Thanks for pointing this out. Revised.

*Comment*

9. *Lines 496-500: The conclusions can be more credible if the author can add some photos of BC particles when discussing the influence of BC's micro-control and mesoporous.*

**Reply**

Thanks for the suggestion. We indeed measured the microporosity and the mesoporosity. The data were presented in Table S4 for better clarity.

## **Anonymous Referee #2**

Received and published: 5 May 2020

### *Comment*

#### **General comments**

*This paper reports on the hygroscopic properties of 15 different types of black carbon (BC) aerosol particles. Both equilibrium and kinetics of water uptake were measured with various methods. The results indicate a fairly wide variation of hygroscopicity amongst the BC types. These variations correlate with the types of dissolved minerals, organic carbon, and soluble ions present with the black carbon. Overall the paper is fairly well-written, with some suggested corrections listed below. A few concerns listed below should be addressed prior to publication.*

### Reply

We appreciate the reviewer's positive comments.

### *Comment*

#### **Specific comments**

*Throughout the paper, be more specific and clear when referring to "black carbon". For example, in the title of the paper, I think you mean to say something like "15 black carbon types". Adding the word "types" at other points in the manuscript are necessary as well (e.g. line 420). You should also clearly define "soot". Why is it not diesel BC or herbal/woody soot?*

### Reply

We appreciate the reviewer's suggestion. The term "black carbon-containing particles (BCPs)" was adopted from the literature to better describe the samples tested in this study.

Following the reviewer's suggestion, we explicitly described the structural and morphological properties of soot (shown as below).

Compared with char and charcoal, soot (another type of BCPs) produced from fossil fuel combustion is comprised of more regular shaped, chain-like agglomerates of primary particles, which consist of perturbed graphitic layers oriented concentrically in an onion-like fashion (Nienow and Roberts, 2006). (Page 5, lines 99-103)

### *Comment*

*Along the lines of the previous comment, I don't think that Line 61 is a completely accurate definition of BC. You reference Bond et al., 2013 in Line 43, so I would assume you would follow their definition. Bond et al., 2013 defines BC as being refractory, insoluble, and consisting of an aggregate of small carbon spherules (among other attributes). Thus, does "BC" really encompass the salts and minerals you mention? (In my opinion, no.)*

## Reply

We understand the reviewer's concern. Please refer to the above reply. A more accurate definition of black carbon was provided according to Bond et al., 2013 (shown as below).

Black carbon (BC) refers to a collective term of refractory and insoluble aggregates of small carbon spherules generated from incomplete combustion of biomass and fossil fuels (Bond et al., 2013). (Page 3, lines 44-46)

## Comment

*Again, going back to my first comment, be more clear and specific in your language. You are measuring the hygroscopicity of BC-containing particles from these various sources and your results show how hygroscopicity changes with different impurities in the BC. Some more details on the 3 soot types should be provided. How long was the household soot on the walls of the oven before collection? How much did this soot have contact with air? In other words, what was the likelihood that other gases not related to the actual combustion were adsorbed to this soot? Please also describe the differences in diesel soot - what do you expect the differences to be simply resulting from collection on a filter versus the walls of the tailpipe? Does the diesel engine have a particulate filter installed? I presume that "# 5" and "# 0" refer to different types of diesel fuel? Please explain.*

## Reply

We appreciate the reviewer's suggestion. Please note that the BCPs were dried at 70 °C under vacuum for 12 h to remove residual water and other adsorbed gasses prior to testing of water vapor adsorption. The major difference among the three soot-type BCPs was that they were produced under different conditions. Some revisions were made to better describe the samples tested in the study (shown as below).

A total of 15 BCPs were tested, including 10 herb-derived BCPs, 2 wood-derived BCPs, and 3 soot-type BCPs. The herbs used for preparation of herbal BCPs were amaranth, peanuts, pea, grass, rice, wheat, corn, millet, sorghum (Nantong, Jiangsu Province, China), and bamboo (Lishui, Zhejiang Province, China), and the woods used for preparation of woody BCPs were red pine and poplar (Lishui, Zhejiang Province, China). The dried and dehydrated biomass was pulverized into a fine powder using a high-speed pulverizer (FW 100, Tianjin Taisite Instrument, China), and pyrolyzed in a muffle furnace under an oxygen-limited conditions. The oven temperature was programmed to increase from 20 to 400 °C in 2 h and maintained at 400 °C for 3 h. The Weifu diesel soot was purchased from Wuxi Weifu Automotive Diesel System Co., Ltd. (Jiangsu Province, China). According to the information provided by the manufacturer, the soot was produced under laboratory conditions by burning diesel (type # 5, China) at 1000 °C and was collected by a diesel particulate

filter (NGK-6000YE) from the exhaust stream at a carbon deposition temperature of 250 °C. The diesel engine soot was collected in outdoor conditions from the freshly discharged exhaust particles on the tailpipe of a diesel truck (Dongfeng, CY4100, 2015, China) equipped with a diesel engine (CY4100Q, 3.7 L, Diesel # 0) and a diesel particulate filter (BST-5L-QCD). The household soot was collected on the inner wall of a stove chamber (Linkou County, Heilongjiang Province, China) 1 hour later after burning of coal and wood for winter cooking and heating under limited oxygen exposure. (Page 6, lines 116-136)

*Comment*

*Line 180 - Please comment on how drying the samples would effect interpretation of your results for ambient BC aerosol.*

*Reply*

Thanks for the suggestion. Please refer to the revision made as follows.

Prior to testing, the BCPs (about 10 mg) were dried at 70 °C under vacuum for 12 h to remove residual water vapor and set a baseline for comparison of water vapor adsorption behaviors among different samples. (Page 9, lines191-194)

*Comment*

*Line 183 - How do you know?*

*Reply*

The amount of water sorbed to the sample tube was measured and showed to be negligible (Page 9, line 194-197).

*Comment*

*Line 227-228 - I do not understand this sentence.*

*Reply*

Please refer to the following revision.

Similarly, the surfaces of all the 15 BCPs were dominated by C and O; however, the differences of the surface C, O compositions among the 15 BCPs were much smaller compared to the bulk C, O compositions. (Page 10-11, lines 239-241)

*Comment*

*Figure 1 - What are the error bars/uncertainty on each datapoint? You talk about the hysteresis in the plots so it is important to establish that the adsorption and desorption curves are statistically different from each other. Also, the way these are plotted, some of the hysteresis is hard to see anyways. On Line 374, not all BC/soot curves are obviously hysteretic, so please specify here.*

Reply

Unlike other experimental data, the data presented in Figure 1 were collected with single-point. It is common to see that desorption isotherms of water vapor to porous media are conducted with single-point (not in replicate). The data of equilibrium water uptake for linear regression were obtained by saturated aqueous salt solutions and collected in duplicate (Figure S5). The error bars for most of the data points are smaller than the symbols.

In the revised version, dash color lines were used to increase discrimination and clarity.

In fact, only some of the herb BCPs and soot samples showed strong hysteresis effect. Please refer to the following revision.

As can be seen from the sorption-desorption isotherms in Figure 1, some herbal BCPs (Amarance, Peanuts, Wheat, Millet, Pea, and Sorghum) and soot (Diesel engine soot and Household soot) showed strong hysteresis effect (irreversible sorption), whereas none of the woody BCPs showed hysteresis effect. (Page 19, lines 402-405)

Comment

*Line 327 - The results at 84% humidity are not shown anywhere in the paper or supplemental. Please add.*

Reply

Thanks for pointing this out. Please refer to the revision made as follows for better clarity.

The regression accuracy ( $R^2$  and  $P$ ) values at the 7 different RH levels (23, 33, 43, 47, 75, 84, 94%) are summarized in Table S8. (Page 16, lines 341-343)

Comment

*Line 330 - Is the weak correlation simply due to lower signals?*

Reply

Not really. The data of equilibrium water uptake could be accurately measured even at low humidity levels. As seen from Figure S5, most of the error bars are smaller than the symbols.

Comment

*Line 334 - The OC constituents in which BC type? Can you point to specifics in Table 1 at this point in the paper as well?*

Reply

Thanks for pointing this out. Please refer to the revision as follows.

As indicated by the elemental analysis results (Table S2), the OC constituents in the three representative BCPs (Grass, Red pine, and Household soot) contained large amounts of oxygen-containing groups, which expectedly had very high hygroscopicity (Xiao et al., 2013). (Page 17, lines 353-356)

*Comment*

*Figure 2 - Rather than look at each constituent individually, what about a multi-factor approach, similar to Positive Matrix Factorization (PMF)? If it is always true, for example, that several of your compositional properties are always correlated, then separating them as you do in Figure 2 does not actually reveal any new information. You have plenty of data in this study to feed into a multi-factor analysis, and I think you may learn quite a bit from that type of analysis.*

*Reply*

We appreciate the reviewer's suggestion. Indeed, a better correlation relationship could be obtained by binary factor linear regression. Please refer to the following revision.

The above one-factor linear correlation analysis indicated that at high RH the hygroscopicity of BCPs was dominated by OC and dissolved minerals. Consistently, a better positive correlation ( $R^2 = 0.90$ ,  $P < 0.0001$ ) could be obtained between the equilibrium water uptake and the contents of  $OC_{TGA}$  and dissolved mineral by binary linear regression for the tested group of BCPs (Figure S8). Interestingly, the correlation relationship became poorer as the RH level gradually increased, and the worst correlation was shown at 23% RH ( $R^2 = 0.21$ ,  $P = 0.028$ ). The results suggested that the hygroscopicity of BCPs at low RH was controlled by different factors. (Page 17-18, lines 365-372)

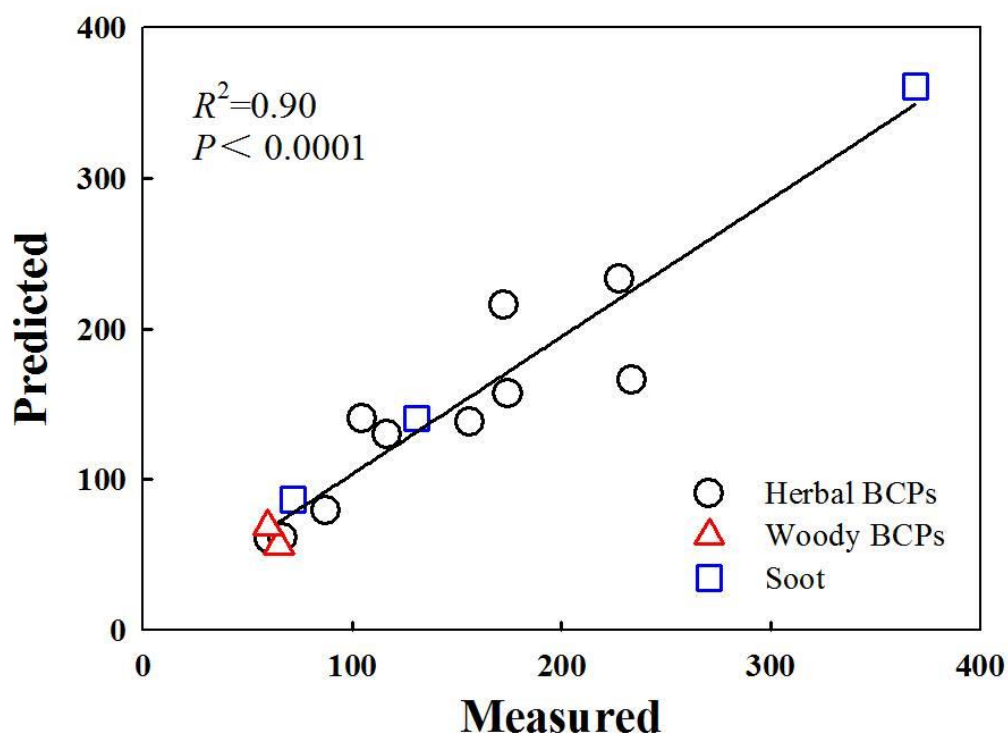


Figure S8. Relationship between measured values of equilibrium water uptake at 94% relative humidity vs. predicted values obtained by binary factor regression based on contents of  $OC_{TGA}$  and dissolved minerals for the group of BCPs. Regression equation:  $Uptake = 9.886OC_{TGA} + 17.459 DM - 16.839$ , where  $OC_{TGA}$  and DM are percentage contents of  $OC_{TGA}$  and dissolved minerals.

*Comment*

Line 369-373 - This seems like a reasonable hypothesis, but the way this section is worded makes it sound like you came up with the hypothesis to fit the results rather than vice-versa. You could cite some literature here to strengthen your arguments and show how your data supports this claim.

Reply

Thanks for the suggestion. Supportive literature references were cited. Please refer to the following revision.

The consistency between the total porosity and the EC content was likely due to the dominant role of graphitized carbons (EC) in forming rigid pore structures of BCPs (Han et al., 2014). (Page 19, lines 395-398)

*Comment*

Figure 3 - Please use the same x-axis limits on parts a, b, and c.

Reply

Revised. Thanks.

*Comment*

*Line 429-430 - Please explain the physical meaning behind a second-order model fitting the data better than a first-order model. Why is this important?*

Reply

We understand the reviewer's concern. Unfortunately, the pseudo-first-order and pseudo-second-order kinetic sorption models are only mathematical formulas for assessing how fast a sorption process approaches its equilibrium state. There are no physical meanings of these models. The pseudo-second order model ( $R^2 > 0.97$ ) fits the data better than the pseudo-first order model, so the pseudo-second-order rate constant ( $k_2$ ) was used for linear regression analysis. Please refer to the following revision for better clarity.

Note that these two kinetic models were applied only for quantitative comparison of apparent sorption kinetics among different BCPs, but not for illustration of sorption mechanisms. (Page 22, lines 458-460)

*Comment*

*Line 458 - Figure 5 shows that EC is also positively correlated, not just total porosity (spelling error there too).*

Reply

Thanks for pointing this out. Please refer to the following revision.

Likewise, a positive correlation ( $R^2 = 0.45$ ,  $P = 0.0061$ ) was observed between the  $k_2$  and the EC content, which could be ascribed to the formation of rigid pore structures dominantly by graphitized carbons (EC) (Han et al., 2014). (Page 24, lines 497-501)

*Comment*

*Line 496-500 - Why aren't there active sites at high humidity conditions?*

Reply

We understand the reviewer's concern. Although these sites could sorb water molecules fast, they had limited contents. Please refer to the following revision.

The fast water uptake kinetics under low humidity conditions was attributed to the binding to high affinity, active sites (OC and salts), which could sorb water vapor fast but had limited contents. (Page 26, lines 532-534)

*Comment*

**Technical corrections**

*Line 25 - I don't understand the use of "BC pool" here.*

Reply

It was changed to “group of BCPs” to avoid confusion.

*Comment*

*Line 42 - Is recalcitrant the right word to use here?*

Reply

The term “BC” was redefined according to the literature study by Bond et al., 2013. Please refer to the following revision.

Black carbon (BC) refers to a collective term of refractory and insoluble aggregates of small carbon spherules generated from incomplete combustion of biomass and fossil fuels (Bond et al., 2013) (Page 3, lines 44-46)

*Comment*

*There are several uses of "this" as the subject/noun in your sentences. Please be more clear in your writing. There are a few other typos, missing "-s" or "the", missing spaces in captions, etc., throughout the paper. Give it another careful proofread before publication. Be consistent on whether using past or present tense.*

Reply

Thanks for pointing this out. We carefully read the paper and made corresponding revisions.

1 An investigation on hygroscopic properties of 15 black carbon  
2 (BC)-containing particles from different carbon sources: Roles  
3 of organic and inorganic components

4  
5 Minli Wang<sup>a</sup>, Yiqun Chen<sup>a</sup>, Heyun Fu<sup>a</sup>, Xiaolei Qu<sup>a</sup>, Bengang Li<sup>b</sup>, Shu Tao<sup>b</sup>, and  
6 Dongqiang Zhu<sup>a,b,\*</sup>

7 <sup>a</sup> State Key Laboratory of Pollution Control and Resource Reuse, School of the  
8 Environment, Nanjing University, Jiangsu 210046, China

9 <sup>b</sup> School of Urban and Environmental Sciences, Key Laboratory of the Ministry of  
10 Education for Earth Surface Processes, Peking University, Beijing 100871, China

11

12

13 Manuscript prepared for *Atmospheric Chemistry and Physics*

14 <sup>\*</sup>Corresponding author. Tel.: +86 010-62766405. E-mail: zhud@pku.edu.cn (D. Zhu)

## 15 Abstract

16 The hygroscopic behavior of black carbon (BC)-containing particles (BCPs) has a  
17 significant impact on global and regional climate change. However, the mechanism  
18 and factors controlling the hygroscopicity of BCPs from different carbon sources are  
19 not well understood. Here, we systematically measured the equilibrium and kinetics of  
20 water uptake by 15 different BCPs (10 herb-derived BCPs, 2 wood-derived BCPs, and  
21 3 soot-type BCPs) using gravimetric water vapor sorption method combined with  
22 in-situ diffuse reflectance infrared Fourier transform spectroscopy (DRIFTS). In the  
23 gravimetric analysis, the sorption/desorption equilibrium isotherms were measured  
24 under continuous-stepwise water vapor pressure conditions, while the kinetics was  
25 measured at a variety of humidity levels obtained by different saturated aqueous salt  
26 solutions. The equilibrium water uptake of the tested group of BCPs at high relative  
27 humidity (> 80%) positively correlated to the dissolved mineral content (0.01–13.0  
28 wt%) ( $R^2 = 0.86$ ,  $P = 0.0001$ ), the content of the thermogravimetrically analyzed  
29 organic carbon ( $OC_{TGA}$ , 4.48–15.25 wt%) ( $R^2 = 0.52$ ,  $P = 0.002$ ), and the content of  
30 the alkali-extracted organic carbon ( $OC_{AE}$ , 0.14–8.39 wt%) ( $R^2 = 0.80$ ,  $P = 0.0001$ ). In  
31 contrast, no positive correlation was obtained with the content of total organic carbon  
32 or elemental carbon. Among the major soluble ionic constituents, chloride and  
33 ammonium were each correlated with the equilibrium water uptake at high relative  
34 humidity. Compared with the herbal BCPs and soot, the woody BCPs had much lower  
35 equilibrium water uptake, especially at high relative humidity, likely due to the very  
36 low dissolved mineral content and OC content. The DRIFTS analysis provided  
37 generally consistent results at low relative humidity. The kinetics of water uptake  
38 (measured by pseudo-second-order rate constant) correlated to the content of  $OC_{TGA}$   
39 and  $OC_{AE}$  as well as the content of chloride and ammonium at low relative humidity

40 (33%), but to the porosity of BCPs at high relative humidity (94%). This was the first  
41 study to show that BCPs of different types and sources had greatly varying  
42 hygroscopic properties.

### 43 1. Introduction

44 Black carbon (BC) refers to a collective term of refractory and insoluble aggregates of  
45 small carbon spherules generated from incomplete combustion of biomass and fossil  
46 fuels (Bond et al., 2013). BC-containing particles (BCPs) are ubiquitous in the  
47 atmosphere and are a major component of atmospheric carbonaceous aerosols  
48 (Schwarz et al., 2008). Due to the strong ability to absorb visible light (Yuan et al.,  
49 2015), BCPs cause positive radiative forcing effects on climate and are considered an  
50 important factor driving global warming (Matthews et al., 2009). Once immersed into  
51 cloud droplets, BCPs can also facilitate water evaporation and cloud dispersion via  
52 enhanced absorption of solar radiation, and thus produce indirect radiative forcing  
53 effects (Powelson et al., 2014). Additionally, the large specific surface area of BCPs  
54 creates a potential for heterogeneous reactions with trace gases (such as volatile  
55 halocarbons) in the atmosphere (Qiu et al., 2012), therefore heavily impacting  
56 atmospheric chemistry and air quality. Hygroscopicity is a key determinant of  
57 physical, chemical, and optical properties of BCPs by changing particle size, phase  
58 state, and quality and morphological development, which in turn affect aerosol  
59 radiation effect, formation of cloud and ice nuclei, and heterogeneous chemical  
60 reactions (Bond et al., 2013; Liu et al., 2018). Furthermore, the hygroscopicity of  
61 BCPs is an important factor contributing to the risk of human respiratory infections,  
62 cardiovascular diseases, and other infectious diseases (Haddrell et al., 2015).

63 Inherited from parent carbon source or produced from combustion process, large  
64 content of inorganic impurities are often present in BCPs, consisting of a variety of

65 amorphous or crystalline salts (sulfates, chlorides, etc.) as well as semi-crystalline  
66 minerals (such as silica) (Stanislav et al., 2013). Despite the relatively low content, the  
67 inorganic components play in **BCPs** a significant role in water uptake, depending on  
68 their types, contents, and mixing ratios (Lewis et al., 2009). As the factors and  
69 processes governing the hygroscopic deliquescence of inorganic salts are very  
70 complicated (Reid et al., 2005; Zhang et al., 2012), it is of a great challenge to assess  
71 the contribution of a specific salt to the overall hygroscopicity of **BCPs**, and thus, its  
72 role is still controversial. Previous studies suggested that KCl was responsible for the  
73 high hygroscopicity of **BCPs** produced by fresh biomass burning (Posfai et al., 2003),  
74 while the presence of  $K_2SO_4$  or  $KNO_3$  caused the low hygroscopicity of **BCPs**  
75 produced by aged biomass burning (Li et al., 2003).

76 The organic components in **BCPs** consist of graphitized elemental carbon (EC) and  
77 non-condensed, amorphous organic carbon (OC) (Lian and Xing, 2017). The  
78 contribution of EC to the overall hygroscopicity of **BCPs** is considered low due to the  
79 very high hydrophobicity (Seisel et al., 2005). The role of OC in the hygroscopic  
80 growth of **BCPs** is intricate and debatable. The positive effect of OC is mainly  
81 attributed to water absorption by the oxygen-containing functional groups (Fletcher et  
82 al., 2007; Suda et al., 2014). The negative effect of OC is suggested to stem from the  
83 impeded mass transfer process of water molecules by formation of coatings on  
84 hygroscopic minerals or inhomogeneous morphology inside the particle (Sjogren et al.,  
85 2007; Stemmler et al., 2008). In addition to the total content, the molecular weight,  
86 water solubility, surface tension, and type and content of functional groups of OC  
87 were all found to influence the overall hygroscopicity of **BCPs**. Moreover, the effect  
88 of OC on **BCPs** hygroscopicity is further complicated by the formation of organic  
89 minerals (presumably through strong covalent bonds) (Archanjo et al., 2014; Reid et

90 al., 2005; Zuend et al., 2011).

91 The carbon sources for BCPs released into the atmosphere are expected to be highly  
92 diversified and cover a wide range of plant biomass, coals, and refined oil products,  
93 although their quota can hardly be accurately assessed (Andreae and Gelencser, 2006).  
94 The chemical compositional, structural, and morphological properties of BCPs depend  
95 significantly on carbon sources and combustion conditions (Xiao et al., 2018). For  
96 instance, crop residue-derived biochar often has higher mineral content than  
97 wood-derived charcoal, while biochar formed at higher pyrolysis temperatures  
98 generally have higher aromaticity, specific surface area, and pore volume but lower  
99 polarity than biochar formed at lower temperatures (Wei et al., 2019). Compared with  
100 char and charcoal, soot (another type of BCPs) produced from fossil fuel combustion  
101 is comprised of more regular shaped, chain-like agglomerates of primary particles,  
102 which consist of perturbed graphitic layers oriented concentrically in an onion-like  
103 fashion (Nienow and Roberts, 2006). Previous studies on hygroscopicity of BCPs  
104 have mainly focused on wood-derived BCPs (Carrico et al., 2010; Day et al., 2006),  
105 whereas BCPs from other carbon sources has been largely overlooked. It remains  
106 unclear whether BCPs from different carbon sources would differ significantly in  
107 hygroscopicity.

108 Herein we systematically investigated the equilibrium and kinetics of water uptake  
109 by 15 different BCPs derived from wood, herb, coal, and diesel at varying relative  
110 humidity (RH) levels by gravimetric sorption and in-situ diffuse reflectance infrared  
111 Fourier transform spectroscopy (DRIFTS). The chemical, compositional, and  
112 structural properties of the tested group of BCPs were thoroughly characterized to  
113 unveil the key factors controlling the hygroscopic properties.

## 114 2. Experimental methods

## 115 **2.1. Preparation of BCPs**

116 A total of 15 BCPs were tested, including 10 herb-derived BCPs, 2 wood-derived  
117 BCPs, and 3 soot-type BCPs. The herbs used for preparation of herbal BCPs were  
118 amaranth, peanuts, pea, grass, rice, wheat, corn, millet, sorghum (Nantong, Jiangsu  
119 Province, China), and bamboo (Lishui, Zhejiang Province, China), and the woods  
120 used for preparation of woody BCPs were red pine and poplar (Lishui, Zhejiang  
121 Province, China). The dried and dehydrated biomass was pulverized into a fine  
122 powder using a high-speed pulverizer (FW 100, Tianjin Taisite Instrument, China),  
123 and pyrolyzed in a muffle furnace under an oxygen-limited conditions. The oven  
124 temperature was programmed to increase from 20 to 400 °C in 2 h and maintained at  
125 400 °C for 3 h. The Weifu diesel soot was purchased from Wuxi Weifu Automotive  
126 Diesel System Co., Ltd. (Jiangsu Province, China). According to the information  
127 provided by the manufacturer, the soot was produced under laboratory conditions by  
128 burning diesel (Diesel # 5, China) at 1000 °C and was collected by a diesel particulate  
129 filter (NGK-6000YE) from the exhaust stream at a carbon deposition temperature of  
130 250 °C. The diesel engine soot was collected in outdoor conditions from the freshly  
131 discharged exhaust particles on the tailpipe of a diesel truck (Dongfeng, CY4100,  
132 2015, China) equipped with a diesel engine (CY4100Q, 3.7 L, Diesel # 0) and a diesel  
133 particulate filter (BST-5L-QCD). The household soot was collected on the inner wall  
134 of a stove chamber (Linkou County, Heilongjiang Province, China) 1 hour later after  
135 burning of coal and wood for winter cooking and heating under limited oxygen  
136 exposure. The obtained samples of BCPs were further ground to pass a 100-mesh  
137 sieve (0.15 mm) and stored sealed in a brown glass bottle at 4 °C.

## 138 **2.2. Characterization of BCPs**

139 Elemental analysis (EA) was performed using a Vario micro cube elemental analyzer

140 (Elementar, Hanau, Germany). Surface elemental compositions were measured by  
141 X-ray photoelectron spectroscopy (XPS) (PHI 5000 VersaProbe, UIVAC-PHI, Japan).  
142 Mineral compositions were measured by X-ray fluorescence (XRF) (ARL-9800, ARL  
143 Corporation, Switzerland). Fourier-transform infrared (FTIR) spectra were recorded  
144 on a Bruker Tensor 27 Karlsruhe spectrometer (Germany) using KBr pellets in the  
145 range of 400 to 4000  $\text{cm}^{-1}$ . X-ray diffraction (XRD) spectra were recorded on an AXS  
146 D8 Advance spectrometer (Germany) using Cu  $K\alpha$  radiation at a  $2\theta$  angle ranging  
147 from 5 to 70°. Raman spectra were collected on a Horiba Jobin Yvon LabRam  
148 HR-800 spectrometer equipped with a 514 nm laser (France).  $\text{N}_2$  adsorption isotherms  
149 to the 15 BCPs were obtained on a Micromeritics ASAP 2020 (Micromeritics  
150 Instrument Co., Norcross, GA, USA) apparatus at  $-196^\circ\text{C}$  (77 K).

151 Three different methods, thermogravimetric analysis (TGA), alkali extraction, and  
152 water extraction, were explored to quantify the content of OC in BCPs (referred to as  
153  $\text{OC}_{\text{TGA}}$ ,  $\text{OC}_{\text{AE}}$ , and  $\text{OC}_{\text{WE}}$ , respectively). The content of  $\text{OC}_{\text{TGA}}$  was measured as the  
154 weight loss during the heating of BCPs from 30 to 300  $^\circ\text{C}$  at a ramp of 10  $^\circ\text{C}$  per  
155 minute in a nitrogen flow (Han et al., 2013) using a TGA 8000 analyzer (PerkinElmer,  
156 USA). To measure the content of  $\text{OC}_{\text{AE}}$ , the sample of BCPs was mixed with 0.1 M  
157 NaOH at a solid-to-solution ratio of 1: 10 (w/w) and magnetically stirred for 12 h,  
158 followed by filtration through a 0.45- $\mu\text{m}$  filter membrane (Pall, USA) (Song et al.,  
159 2002). The filtrate was collected and acidified (pH 1.0 with 6 M HCl), and the total  
160 organic carbon (TOC) content of the sample was measured by a TOC analyzer  
161 (TOC-5000A, Shimadzu, Japan). For the three selected BCPs (Grass, Wheat, and  
162 Household soot), the precipitates formed by acidification were further separated by  
163 centrifugation and dialyzed in deionized (DI) water by dialysis bag (500 Da, Union  
164 Carbide, USA) until no chloride ion was detected by  $\text{AgNO}_3$ , and then freeze-dried.

165 The elemental compositions of the three prepared OC<sub>AE</sub> were measured by EA. To  
166 measure the content of OC<sub>WE</sub> and dissolved minerals, the suspended **BCPs** in DI  
167 water (**BCPs**-to-water ratio of 1: 10, w/w) was sonicated in a water bath for several  
168 minutes, and the mixture was filtered through a 0.45- $\mu$ m membrane. The  
169 **suspension/sonication** procedure was repeated for 6 times. The filtrate was collected  
170 and subjected to TOC analysis to obtain the content of OC<sub>WE</sub>. The concentrations of  
171 ionic constituents (Cl<sup>-</sup>, NO<sub>3</sub><sup>-</sup>, PO<sub>4</sub><sup>3-</sup>, SO<sub>4</sub><sup>2-</sup>, F<sup>-</sup>, COO<sup>-</sup>, C<sub>2</sub>O<sub>4</sub><sup>2-</sup>, Na<sup>+</sup>, NH<sub>4</sub><sup>+</sup>, K<sup>+</sup>, Mg<sup>2+</sup>,  
172 Ca<sup>2+</sup>, Al<sup>3+</sup>) in the filtrate were measured using a  
173 Dionex ICS-1100 ion chromatography (Thermo Scientific, USA). The cations were  
174 eluted using 20 mM methanesulfonic acid on a Dionex IonPac CS12A column (4  $\times$   
175 250 mm), while the anions were eluted using an eluent of 4.5 mM Na<sub>2</sub>CO<sub>3</sub> and 0.81  
176 mM NaHCO<sub>3</sub> on a Dionex IonPac AS14A column (4  $\times$  250 mm). The filtrate was  
177 further freeze-dried and baked at 600  $^{\circ}$ C for 6 h to remove organic components. The  
178 remaining ash was weighed to determine the content of dissolved minerals in **BCPs**. A  
179 portion of the ash was extracted three times using DI water at a solid-to-solution ratio  
180 of 1:10 (w/w) under sonication, and the salinity of the extract was measured by a  
181 ST3100C conductivity meter (OHAUS, USA). All reagents and chemicals used  
182 were of analytical reagent grade.

### 183 **2.3. Measurement of hygroscopicity of **BCPs****

184 The hygroscopicity of **BCPs** at varying RH was measured by gravimetric method  
185 combined with in-situ DRIFTS. The water vapor sorption/desorption isotherms to  
186 **BCPs** under a range of continuous-stepwise water vapor pressures were acquired on  
187 a 3H-2000 PW Multi-stations Gravimetric Method Steam Adsorption Instrument  
188 (Beijing, China) at 25  $^{\circ}$ C using an approach similar to that in previous studies (Gu et  
189 al., 2017). The instrument consists of two main parts: a balance chamber to determine

190 the sample mass to an accuracy  $\pm 1 \mu\text{g}$  and a humidity chamber to regulate the water  
191 vapor pressure to the desired value as monitored online by a pressure sensor. Prior to  
192 testing, the BCPs (about 10 mg) were dried at  $70 \text{ }^\circ\text{C}$  under vacuum for 12 h to remove  
193 residual water vapor and set a baseline for comparison of water vapor adsorption  
194 behaviors among different samples. The amount of water sorbed to BCPs was  
195 monitored as the mass difference before and after sorption. The amount of water  
196 sorbed to the sample tube was measured and showed to be negligible ( $< 0.05\%$  of  
197 the amount of water sorbed to BCPs). The water vapor pressures ranging from 10 to  
198 94% RH were applied to the sorption isotherm branch in a stepwise increasing  
199 sequence and to the desorption isotherm branch in a stepwise decreasing sequence.

200 The kinetics of water sorption to BCPs was measured on a 100 mm closed quartz  
201 chamber (Jiangsu Province, China) using a gravimetric method similar to that in  
202 previous studies (Yuan et al., 2014). Approximately 100 mg of BCPs was dried at  
203  $70 \text{ }^\circ\text{C}$  under vacuum for 12 h, weighed in a 10-mL beaker, and placed in a chamber  
204 under controlled humidity conditions based on different saturated aqueous salt  
205 solutions according to ASTM E104-02 (2007). The saturated solutions of  $\text{CH}_3\text{COOK}$ ,  
206  $\text{MgCl}_2$ ,  $\text{K}_2\text{CO}_3$ ,  $\text{LiNO}_3$ ,  $\text{NaCl}$ ,  $\text{KCl}$ , and  $\text{KNO}_3$  provided RH of 23%, 33%, 43%, 47%,  
207 75%, 84%, 94%, respectively at  $25 \text{ }^\circ\text{C}$ . The sample was continuously weighed and  
208 recorded over a period of time (48 h for low humidity and 96 h for high humidity) to  
209 monitor the amount of sorbed water. The RH was monitored in real time using a  
210 Honeywell HIH4000 hygrometer (USA) with measurement variance was less than 5%.  
211 Sorption equilibrium was reached in the late stage of the experiment as evidenced by  
212 the stabilized constant value of sample mass. In addition to kinetic data, sorption  
213 isotherms were also collected for the seven selected RH levels using the measured  
214 mass under equilibrium conditions.

215 Samples of **BCPs** equilibrated at different RH levels were characterized by in situ  
216 DRIFTS using a Bruker Tensor 27 spectrometer equipped with a high-sensitivity  
217 mercury-cadmium-telluride (MCT) detector working under liquid N<sub>2</sub> conditions and a  
218 chamber fitted with ZnSe windows (Harrick Scientific, USA). About 10 mg of **BCPs**  
219 pre-dried at 70 °C under vacuum for 12 h was transferred to the chamber which was  
220 connected to a gas feeding system. The chamber was sealed and purged with  
221 high-purity N<sub>2</sub> at a flow rate of 100 mL per minute for at least 3 h to remove  
222 pre-adsorbed gases on **BCPs** and to minimize the interference of environmental CO<sub>2</sub>.  
223 The humidity in the chamber was regulated by mixing high-purity N<sub>2</sub> and saturated  
224 water vapor at 25 °C with varying ratios and monitored in real time by a hygrometer  
225 (Vaisala Humitter, Australia). The sample was equilibrated with the gas mixture in the  
226 chamber for at least 30 minutes to reach sorption equilibrium based on pre-determined  
227 kinetics. The spectra were acquired by co-adding and averaging a plurality of 500  
228 scans with a resolution of 4 cm<sup>-1</sup> (Song and Boily, 2013). The amount of water sorbed  
229 to **BCPs** was monitored by the integrated intensity of the O-H stretching region from  
230 2750 to 3660 cm<sup>-1</sup> (Ghorai et al., 2011).

### 231 **3. Results and discussion**

#### 232 **3.1. Characteristics of **BCPs****

233 Bulk elemental compositions by EA and surface elemental compositions by XPS are  
234 summarized in Table S1. The bulk elemental compositions of all **BCPs** were  
235 dominated by C and O, together accounting for 54%–96% of the total. However, the  
236 bulk C, O compositions differed significantly among the 15 **BCPs**, ranging from 32 to  
237 76% for C and from 16 to 69% for O. With the exception of the woody **BCPs**, the  
238 differences were apparent within each category of the herbal **BCPs** and the soot.  
239 **Similarly, the surfaces of all the 15 BCPs were dominated by C and O; however, the**

240 differences of the surface C, O compositions among the 15 BCPs were much smaller  
241 compared to bulk C, O compositions. Besides C and O, EA detected low amounts of  
242 N (< 3.7%) and S (< 1.8%), and XPS detected low amounts of N (< 4.3%), Si (<  
243 5.6%), and S (< 0.6%). The contents of oxygen-containing groups in the 15 BCPs  
244 were qualitatively compared by the FTIR spectra (Figure S1). All the tested BCPs  
245 except Weifu diesel soot showed characteristic peaks of esters ( $1700\text{ cm}^{-1}$ ), ketones  
246 ( $1613, 1100\text{ cm}^{-1}$ ), and phenols ( $1270\text{ cm}^{-1}$ ) (Keiluweit et al., 2010), generally with  
247 larger peak intensities observed for herbal BCPs and household soot.

248 Table 1. Chemical, compositional, and pore properties of different BCPs.

BCPs	OC			EC <sup>d</sup> (wt%)	Dissolved minerals (wt%)	Total Porosity <sup>e</sup> (m <sup>3</sup> g <sup>-1</sup> )	SSA <sup>f</sup> (m <sup>2</sup> g <sup>-1</sup> )
	OC <sub>TGA</sub> <sup>a</sup> (wt%)	OC <sub>AE</sub> <sup>b</sup> (wt%)	OC <sub>WE</sub> <sup>c</sup> (wt%)				
Amaranth	6.24	2.6	1.75	25.84	10.8	0.004	0.314
Grass	7.24	2.37	1.01	51.56	4.8	0.008	5.587
Peanuts	7.45	1.78	0.8	41.86	4.2	0.002	0.192
Pea	9.59	1.98	0.09	54.48	3.6	0.005	4.679
Rice	6.81	0.6	0.11	48.06	0.6	0.023	31.88
Wheat	8.25	1.82	0.37	42.65	5.8	0.01	7.382
Millet	9.41	1.97	0.93	32.25	8	0.023	8.319
Corn	6.55	0.14	0.32	46.47	1.8	0.028	28.6
Sorghum	9.09	1.12	0.62	55.26	4.8	0.001	0.192
Bamboo	6.84	0.23	0.12	61.7	0.6	0.029	51.94
Red pine	7.4	0.2	0.05	62.59	0.01	0.032	64.24
Poplar	7.58	0.19	0.09	64.22	0.6	0.071	107.6
Diesel engine soot	9.57	1.4	0.78	27.37	3.6	0.021	6.119
Weifu diesel soot	4.48	0.57	0.13	71.98	3.4	0.484	194.6
Household soot	15.25	8.39	2.24	21.83	13	0.012	7.79

249 <sup>a</sup>Content of organic carbon determined by TGA. <sup>b</sup>Content of alkali-extracted organic  
250 carbon determined by TOC analysis. <sup>c</sup>Content of water-extracted organic  
251 carbon determined by TOC analysis. <sup>d</sup>Determined by subtracting OC<sub>TGA</sub> content from  
252 total organic carbon content by EA. <sup>e</sup>Total pore volume determined by N<sub>2</sub> adsorption  
253 at 0.97 atmosphere pressure. <sup>f</sup>Specific surface area determined by the BET method.

254 Table 1 summarizes the contents of OC (OC<sub>TGA</sub>, OC<sub>AE</sub>, and OC<sub>WE</sub>) of the 15 BCPs  
255 by TGA, alkali extraction, and water extraction, respectively. For a given BCPs, the  
256 contents of the three types of OC differed pronouncedly, with an increasing order of  
257 OC<sub>WE</sub> < OC<sub>AE</sub> < OC<sub>TGA</sub>. The OC content also differed within the tested group of  
258 BCPs, ranging from 0.05 to 2.24wt% for OC<sub>WE</sub>, from 0.14 to 8.39wt% for OC<sub>AE</sub>, and  
259 from 4.48 to 15.25wt% for OC<sub>TGA</sub>. Compared with the EC (graphitized carbon), the  
260 three types of OC are non-condensed, amorphous, and more rich in oxygen-containing  
261 functional groups, which was evidenced by the fact that the OC<sub>AE</sub> from the three  
262 selected BCPs (Grass, Wheat, and Household soot) had markedly higher bulk

263 compositions of O (results presented in Table S2). The EC content in **BCPs** was  
264 roughly assessed by subtracting the  $OC_{TGA}$  content from the total organic carbon  
265 content measured by EA (results presented in Table 1). The calculated EC content  
266 negatively correlated with the  $OC_{AE}$  content ( $R^2 = 0.43$ ,  $P = 0.0079$ ) for the examined  
267 **group of BCPs**. This **relationship** was reasonable as EC was comprised of mature,  
268 thermodynamically stable graphitized carbons, while OC was comprised of the less  
269 mature and less aromatic constituents remaining after pyrolysis. Except for Weifu  
270 diesel soot, the two woody **BCPs** had the highest EC, but the lowest  $OC_{AE}$  and  $OC_{WE}$   
271 among the 15 **BCPs**.

272 The relative abundance of EC in **BCPs** was also assessed by Raman spectroscopy  
273 (Figure S2). The spectra of all the tested **BCPs** were dominated by a D band at  $1340$   
274  $cm^{-1}$  and a G band at  $1580 cm^{-1}$ , which were ascribed to carbon network defects and  
275 the  $E_{2g}$  mode of the graphitized carbon, respectively (Pimenta et al., 2007). Thus, the  
276 ratio of these two bands ( $I_D/I_G$ ) was inversely proportional to the in-plane crystallite  
277 size of graphitized carbons of **BCPs** (Cancado et al., 2006). The  $I_D/I_G$  ratio of the  
278 woody **BCPs** (0.51–0.59) was less than those of the herbal **BCPs** (0.88–1.09) and the  
279 soot (0.77–1.12) (Table S3), suggesting larger sizes of graphitized carbons in the  
280 woody **BCPs, which** was consistent with the results of OC compositions.

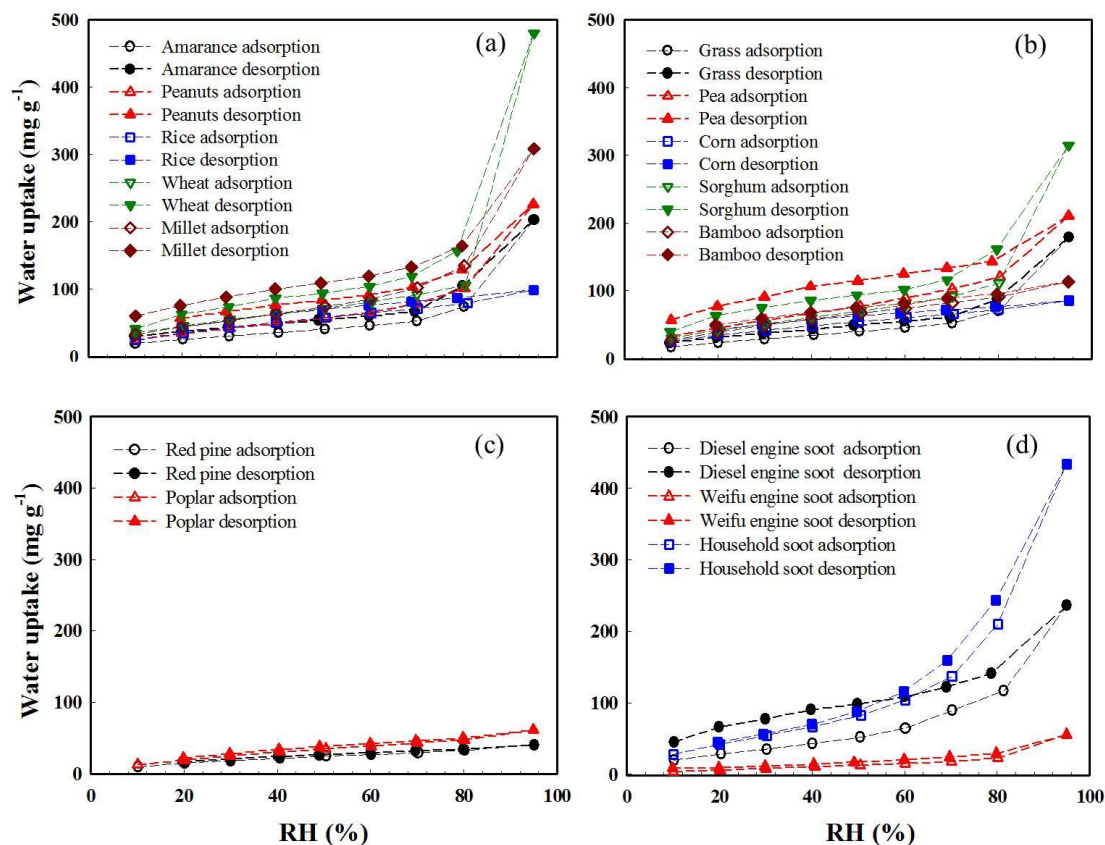
281 The contents of dissolved minerals of the 15 **BCPs** are listed in Table 1, and their  
282 salinities in water extracts are listed in Table S5. The two woody **BCPs** had the lowest  
283 contents of dissolved minerals and salinities, while these contents in **herbal BCPs** and  
284 soot were higher and varied greatly. The mineral compositions characterized by XRF  
285 are listed in Table S6. Si-, K-rich minerals were the two major inorganic constituents  
286 in the herbal **BCPs** and woody **BCPs**. Moreover, these two types of **BCPs** generally  
287 contained trace amounts of S-, Cl-, Ca-, P-, Mg-, Na-, Fe-, and Al-minerals, with

288 lower contents observed for the woody BCPs. The three soot had very different  
289 mineral compositions. Household soot was dominated by S-, Ca-, Si-, and Cl-minerals,  
290 Diesel engine soot was dominated by S-, Ca-, and Fe-minerals, while Weifu diesel  
291 soot contained negligible mineral compositions. As reflected by the observed  
292 characteristic peaks and associated peak intensities in the XRD spectra (Figure S3),  
293 the herbal BCPs and Household soot contained more mineral species with higher  
294 contents than other BCPs, whereas the two woody BCPs and Weifu diesel soot  
295 contained the least species and contents of minerals. Potassium salts, amorphous silica,  
296 and sulfates were the major minerals in the herbal BCPs. Soot had the largest content  
297 of sulfates among the tested BCPs. According to the ion chromatograph analysis  
298 (results presented in Figure S4 and Table S7), the major water-extracted cationic  
299 species from the tested BCPs were  $\text{NH}_4^+$ ,  $\text{K}^+$ , and  $\text{Ca}^{2+}$ , and the major anionic species  
300 were  $\text{SO}_4^{2-}$ ,  $\text{Cl}^-$ , and  $\text{C}_2\text{O}_4^{2-}$ . The herbal BCPs had high contents of  $\text{K}^+$ ,  $\text{C}_2\text{O}_4^{2-}$ , and  $\text{Cl}^-$ ,  
301 while the soot had high content of  $\text{SO}_4^{2-}$ .

302 The Brunauer–Emmett–Teller (BET) specific surface area and total porosity  
303 measured by  $\text{N}_2$  adsorption are also summarized in Table 1. A huge disparity of  
304 specific surface area was shown among the 15 BCPs and among the BCPs within each  
305 category, ranging from 6 to  $200 \text{ m}^2 \text{ g}^{-1}$  for the soot, from 60 to  $110 \text{ m}^2 \text{ g}^{-1}$  for the  
306 woody BCPs, and from 0.1 to  $52 \text{ m}^2 \text{ g}^{-1}$  for the herbal BCPs. The micro- and  
307 mesoporosity of the 15 tested BCPs are summarized in Table S4. The herbal BCPs  
308 and woody BCPs were dominated by micropores (pore size  $< 2 \text{ nm}$ ), which accounted  
309 for more than 50% of the total pore volume. Alternatively, mesopores ( $50 \text{ nm} > \text{pore}$   
310  $\text{size} > 2 \text{ nm}$ ) were the main pore structure of the soot, accounting for more than 61%  
311 of the total pore volume.

### 312 3.2. Hygroscopic properties of BCPs

313 **Equilibrium water uptake.** Figure 1 displays sorption and desorption isotherms of  
314 water vapor with **BCPs** plotted as equilibrium water uptake ( $\text{mg g}^{-1}$ ) by unit mass of  
315 **BCPs** under continuous-stepwise water vapor pressure conditions. Figure S5 displays  
316 the equilibrium sorption isotherms at selected humidity levels obtained by using  
317 saturated aqueous salt solutions. Under similar humidity conditions (80% and 84%),  
318 the water uptake by the 15 **BCPs** was very close between these two humidity  
319 regulation methods (Figure S6), reflecting their technical validity. The woody **BCPs**  
320 showed very different sorption isotherm patterns from the herbal **BCPs** and soot. First,  
321 the water sorbing ability of the woody **BCPs** was much lower. The maximum water  
322 uptake observed at the highest RH (94%) was approximately  $65 \text{ mg g}^{-1}$  by the woody  
323 **BCPs**, but was more than  $400 \text{ mg g}^{-1}$  for the strongest sorbing herbal **BCPs** and soot.  
324 Second, much larger water-uptake disparities were observed within the **group of**  
325 **herbal BCPs** and the soot group than within the **group of woody BCPs**. Additionally,  
326 over the examined RH range (10–94%), the water uptake by the woody **BCPs**  
327 increased slowly and linearly with the RH; however, for the herbal **BCPs** and soot, the  
328 water uptake increased more rapidly with the RH, especially under high humidity  
329 conditions ( $\text{RH} > 70\%$ ).



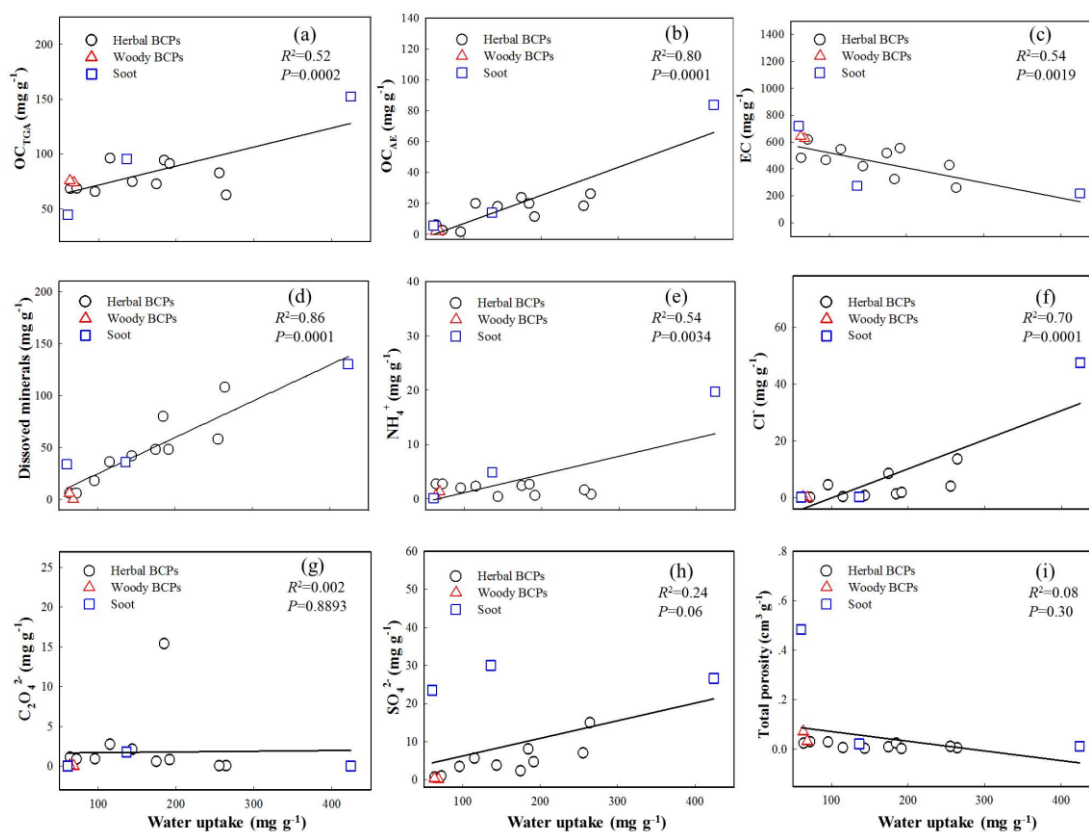
330  
 331 Figure 1. Sorption and desorption isotherms of water vapor plotted as water uptake  
 332 ( $\text{mg g}^{-1}$ ) vs. relative humidity (RH, %) at equilibrium for different BCPs. (a)  
 333 Subgroup 1 of herbal BCPs. (b) Subgroup 2 of herbal BCPs. (c) Woody BCPs. (d)  
 334 Soot. Data were collected with single-point.

335 To better understand the underlying mechanisms and factors controlling the  
 336 hygroscopic properties of BCPs, linear relationships were built between the  
 337 equilibrium water uptake and a wide variety of compositional and pore property  
 338 parameters of the whole group of BCPs. Figure 2 displays regression relationships  
 339 with contents of  $\text{OC}_{\text{TGA}}$ ,  $\text{OC}_{\text{AE}}$ , EC, dissolved minerals, major ionic species ( $\text{NH}_4^+$ ,  $\text{Cl}^-$ ,  
 340  $\text{SO}_4^{2-}$ , and  $\text{C}_2\text{O}_4^{2-}$ ), and total porosity, respectively at 94% RH. The regression  
 341 relationships at 23% RH were presented in Figure S7. The regression accuracy ( $R^2$   
 342 and  $P$ ) values at the 7 different RH levels (23, 33, 43, 47, 75, 84, 94%) are  
 343 summarized in Table S8. Good positive correlations existed between the water uptake

344 and the contents of OC<sub>TGA</sub>, OC<sub>AE</sub>, and dissolved minerals under high humidity  
345 conditions (Figure 2a-d). The highest regression accuracy values obtained were  $R^2 =$   
346  $0.82$ ,  $P < 0.0001$  for OC<sub>TGA</sub> at 84% RH,  $R^2 = 0.80$ ,  $P = 0.001$  for OC<sub>AE</sub> at 94% RH,  
347 and  $R^2 = 0.86$ ,  $P = 0.0001$  for dissolved minerals at 94% RH. However, the  
348 correlations with these constituents became much weaker under low humidity  
349 conditions ( $R^2 = 0.10$ – $0.32$ ,  $P = 0.247$ – $0.028$  at RH = 23%). It can be concluded that  
350 the hygroscopicity of herbal BCPs and soot under high humidity conditions was  
351 mainly controlled by the contents of OC and dissolved minerals. On the other hand,  
352 the low water sorbing ability of the woody BCPs was due to the very low contents of  
353 these constituents. As indicated by the elemental analysis results, the OC constituents  
354 in the three representative BCPs (Grass, Red pine, and Household soot) contained  
355 large amounts of oxygen-containing groups (Table S2), which expectedly had very  
356 high hygroscopicity (Xiao et al., 2013). The very strong water retention ability of  
357 dissolved minerals in BCPs was understandable due to the strong hydration of mineral  
358 surfaces and ionic constituents. No correlation was observed between the water  
359 uptake of BCPs and the total organic carbon content within the whole examined RH  
360 range. Notably, a negative correlation was observed with the EC content (Figure 2c),  
361 especially under high humidity conditions ( $R^2 = 0.54$ ,  $P = 0.0019$  at 94% RH).  
362 Compared with the OC in BCPs, the EC was comprised mainly of hydrophobic fused  
363 aromatic hydrocarbons and had much lower amounts of oxygen-containing groups,  
364 resulting in the very low water sorbing ability.

365 The above one-factor linear correlation analysis indicated that at high RH the  
366 hygroscopicity of BCPs was dominated by OC and dissolved minerals. Consistently, a  
367 better positive correlation ( $R^2 = 0.90$ ,  $P < 0.0001$ ) could be obtained between the  
368 water uptake and the contents of OC<sub>TGA</sub> and dissolved mineral by binary linear

369 regression for the tested group of BCPs (Figure S8). Interestingly, the correlation  
 370 relationship became poorer as the RH level gradually decreased, and the worst  
 371 correlation was shown at 23% RH ( $R^2 = 0.21$ ,  $P = 0.028$ ). The results suggested that  
 372 the hygroscopicity of BCPs at low RH was controlled by different factors.



373  
 374 Figure 2. Relationships between equilibrium water uptake (mg g<sup>-1</sup>) vs. compositional  
 375 and pore property parameters for the group of BCPs at 94% relative humidity. (a)  
 376 TGA-measured organic carbon (OC<sub>TGA</sub>). (b) Alkali-extracted organic carbon (OC<sub>AE</sub>).  
 377 (c) Elemental carbon (EC). (d) Dissolved minerals. (e) Ammonium (NH<sub>4</sub><sup>+</sup>). (f)  
 378 Chloride (Cl<sup>-</sup>). (g) Oxalate (C<sub>2</sub>O<sub>4</sub><sup>2-</sup>). (h) Sulfate (SO<sub>4</sub><sup>2-</sup>). (i) Total porosity.

379 At 94% RH, relatively good positive correlations were observed with NH<sub>4</sub><sup>+</sup> and Cl<sup>-</sup>  
 380 ( $R^2 = 0.50$ – $0.70$ ,  $P = 0.0001$ – $0.0034$ ), but not with SO<sub>4</sub><sup>2-</sup> ( $R^2 = 0.24$ ,  $P = 0.06$ ) or  
 381 C<sub>2</sub>O<sub>4</sub><sup>2-</sup> ( $R^2 = 0.002$ ,  $P = 0.89$ ) (Figure 2e-h). No correlation ( $R^2 = 0.08$ ,  $P = 0.3$ ) was  
 382 observed with the total porosity of BCPs at 94% RH (Figure 2i). Consistently,

383 previous studies reported that chloride salts in biomass burning aerosols had high  
384 hygroscopicity (Jing et al., 2017; Posfai et al., 2003). The poor correlation observed  
385 for  $\text{SO}_4^{2-}$  was ascribed to the low hygroscopicity of  $\text{CaSO}_4$  and  $\text{K}_2\text{SO}_4$ , as evidenced  
386 by their very high deliquescent relative humidity (96–97%) (Freney et al., 2007;  
387 Preturlan et al., 2019). It is noteworthy that the content of  $\text{SO}_4^{2-}$  positively correlated  
388 with the contents of  $\text{Ca}^{2+}$  ( $R^2 = 0.74$ ,  $P < 0.0001$ ) and  $\text{K}^+$  ( $R^2 = 0.69$ ,  $P = 0.0008$ ) for  
389 the tested BCPs. On the other hand, the poor correlation observed for  $\text{C}_2\text{O}_4^{2-}$  was  
390 likely due to the formation of less water-soluble compounds (e.g.,  $\text{CaC}_2\text{O}_4$  and  
391  $\text{H}_2\text{C}_2\text{O}_4$ ) that might depress the hygroscopicity (Buchholz and Mentel, 2008).

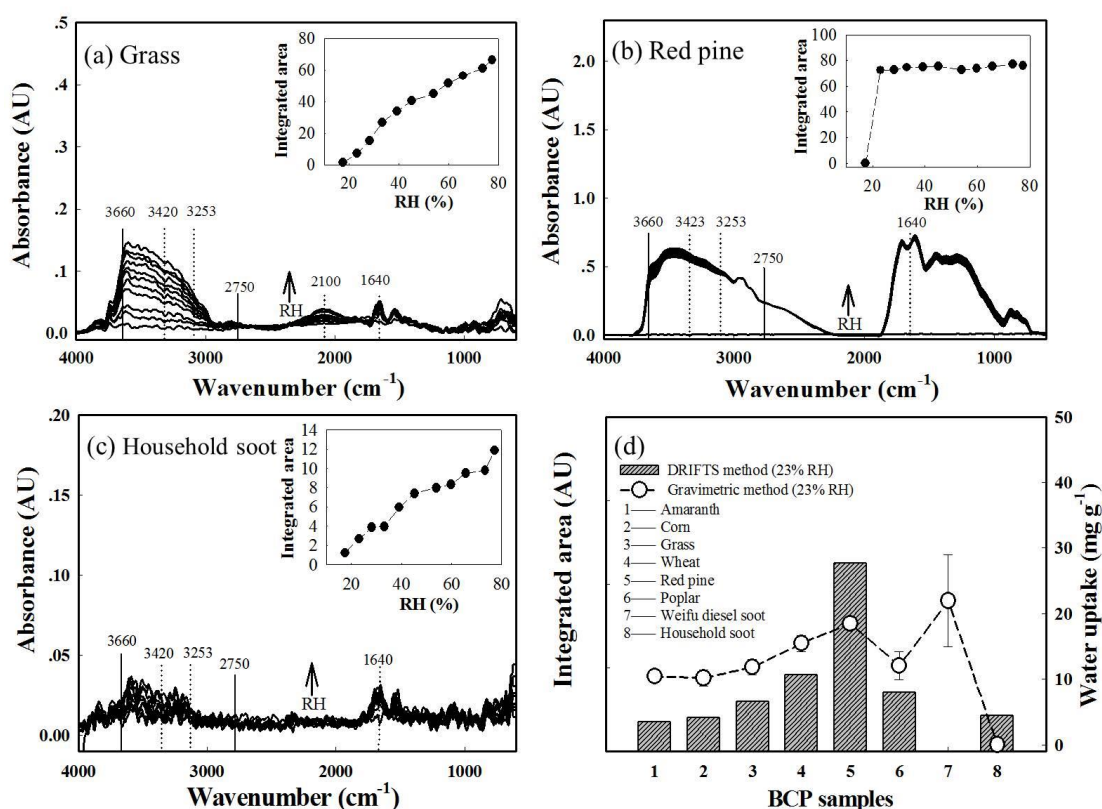
392 The positive correlations observed with  $\text{NH}_4^+$  and  $\text{Cl}^-$  at 94% RH disappeared at  
393 23% RH. Alternatively, a relative good negative correlation ( $R^2 = 0.42$ ,  $P = 0.0095$ )  
394 with the total porosity was shown at 23% RH (Figure S7i). Similarly, a weak negative  
395 correlation ( $R^2 = 0.21$ ,  $P = 0.083$ ) was shown with the EC content at 23% RH. The  
396 consistency between the total porosity and the EC content was likely due to the  
397 dominant role of graphitized carbons (EC) in forming rigid pore structures of BCPs  
398 (Han et al., 2014). On the contrary, a weak positive correlation ( $R^2 = 0.32$ ,  $P = 0.028$ )  
399 was observed between the water uptake and the  $\text{OC}_{\text{TGA}}$  content at 23% RH, indicating  
400 that the OC constituents were an important factor contributing to the overall water  
401 uptake by BCPs under low humidity conditions.

402 As can be seen from the sorption-desorption isotherms in Figure 1, some herbal  
403 BCPs (Amarance, Peanuts, Wheat, Millet, Pea, and Sorghum) and soot (Diesel engine  
404 soot and Household soot) showed strong hysteresis effect (irreversible sorption),  
405 whereas none of the woody BCPs showed hysteresis effect. Irreversible sorption  
406 would lower the release of sorbed water molecules from BCPs in the atmosphere  
407 when the RH changes from a high level to a low level. The observed hysteresis effect

408 of herbal **BCPs** and soot likely stemmed from their relatively high contents of OC  
409 and/or dissolved minerals (such as **Wheat** and Household soot). Sorbing water  
410 molecules could cause strong and irreversible hydration of organic acids (Petters et al.,  
411 2017) and dissolution or phase change of minerals (Adapa et al., 2018), consequently  
412 leading to hysteresis effect due to non-identical structures of **BCPs** between the  
413 sorption and desorption branches even at the same RH. The negligible hysteresis  
414 effect observed on the two woody **BCPs** could be attributed to their very low contents  
415 of OC and dissolved minerals.

416 The equilibrium water uptake by **BCPs** was further investigated by DRIFTS. The  
417 spectra of representative **BCPs** (Grass, Red pine, and Household soot) at varying RH  
418 are presented in Figure 3a-c. Figure 3d compares the water uptake at 23% RH  
419 monitored by the integrated intensity of the O-H stretching region from 2750 to 3660  
420  $\text{cm}^{-1}$  (Ghorai et al., 2011), along with the water uptake measured by the  
421 multi-station gravimetric method for 8 selected **BCPs**. The identified bands of sorbed  
422 water molecules included a combination mode of symmetric stretch around  $3423 \text{ cm}^{-1}$   
423 and asymmetric stretch stretch around  $3253 \text{ cm}^{-1}$  (Gustafsson et al., 2005). The broad  
424 feature peak centered at  $2100 \text{ cm}^{-1}$  was assigned to a combined band of bending,  
425 libration, and hindered translation modes of water, while the peak centered at  $1640$   
426  $\text{cm}^{-1}$  was attributed to the bending mode of water (Ma et al., 2010). The intensities of  
427 these peaks/bands increased with increasing RH. As assessed by the integrated  
428 intensity of the O-H stretching region (see insets in Figure 3a-c), the water uptake by  
429 Grass and Household soot increased gradually with RH from 12 to 80%; however, the  
430 water uptake by Red pine rapidly reached saturation at about 28% RH, and kept  
431 constant when the RH was further increased. With the exception of Weifu diesel soot,  
432 the disparity pattern of water uptake by the 8 selected **BCPs** at 23% RH monitored by

433 DRIFTS was similar to that monitored by the multi-station gravimetric method  
 434 (Figure 3d). However, the disparities were very large between these two methods at  
 435 80% RH (Figure S9), which was probably because the saturated effect encountered in  
 436 detection of sorbed water molecules by FTIR (Gustafsson et al., 2005) became worse  
 437 under high humidity conditions. Moreover, the DRIFTS signals of sorbed water  
 438 molecules might be influenced by the distribution of sorption sites (e.g., minerals vs.  
 439 OC and exterior vs. interior), and the caused effects might lead to larger deviations  
 440 under high humidity conditions.



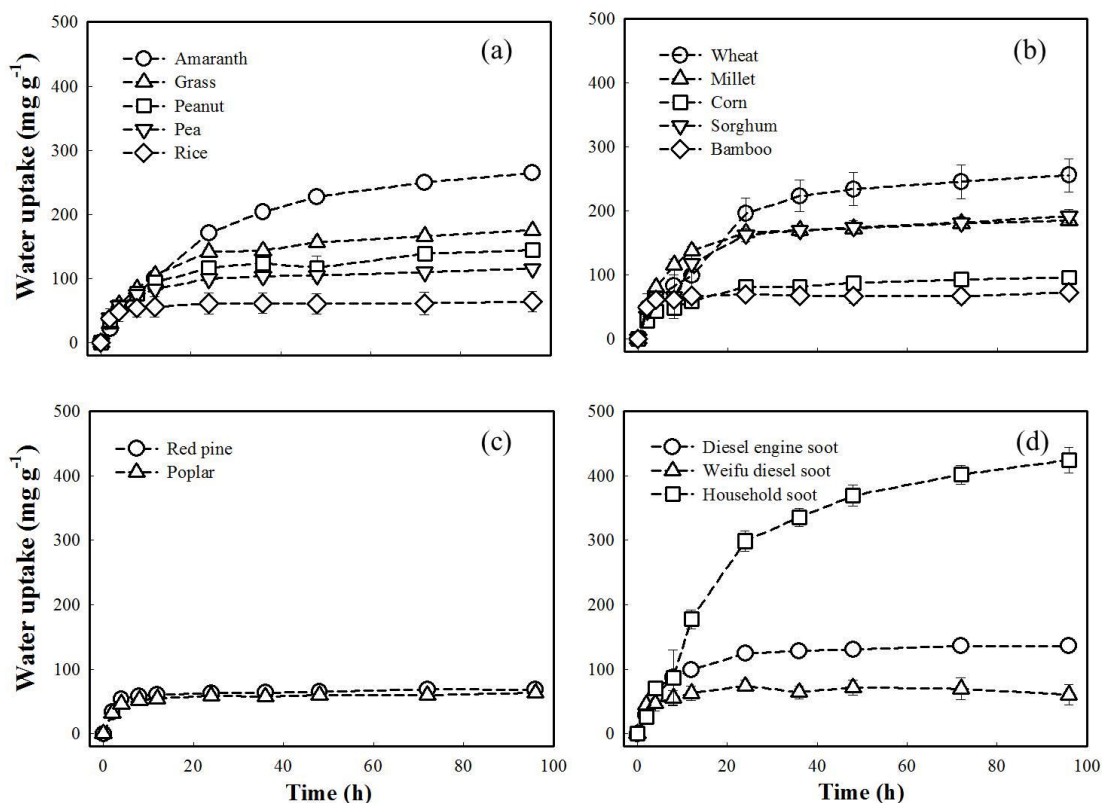
441

442 Figure 3. Diffuse reflectance infrared Fourier transform spectroscopy (DRIFTS)  
 443 characterization of equilibrium water uptake by BCPs. (a-c) Spectra for the three  
 444 representative BCPs (Grass, Red pine, and Household soot) equilibrated at varying  
 445 relative humidity (RH) levels. (d) Comparison of equilibrium water uptake measured  
 446 as integrated area of O-H stretching region (2750–3660 cm<sup>-1</sup>) between 8 selected

447 BCPs at 23% relative humidity. Error bars represent standard variations from  
448 duplicate samples. Insets in subfigures (a-c) present water uptake measured as  
449 integrated area of O-H stretching region against RH.

450 **Kinetic water uptake.** Figure 4 displays the water vapor sorption kinetics to the 15  
451 BCPs at 94% RH obtained by saturated aqueous salt solutions. The sorption kinetics  
452 at 33% RH was presented in Figure S10. The two woody BCPs exhibited similar  
453 kinetics curves; however, the herbal BCPs and soot showed very different kinetic  
454 patterns within each group. The kinetic data were fitted to the pseudo-first-order and  
455 pseudo-second-order models,  $dq_t/dt = k_1 (q_e - q_t)$  and  $dq_t/dt = k_2 (q_e - q_t)^2$ , respectively,  
456 where  $q_t$  was the sorbed concentration at time  $t$ ,  $q_e$  was the equilibrium sorbed  
457 concentration, and  $k_1$  and  $k_2$  were the pseudo-first-order and pseudo-second-order rate  
458 constants, respectively. Note that these two kinetic models were applied only for  
459 quantitative comparison of apparent sorption kinetics among different BCPs, but not  
460 for illustration of sorption mechanisms. The fitting parameters ( $q_e$ ,  $k_1$ ,  $k_2$ ) for the three  
461 selected RH levels (33, 47, and 94%) are summarized in Tables S9-S10. The  
462 pseudo-second-order model ( $R^2 > 0.97$ ) fits the data better than the pseudo-first-order  
463 model ( $R^2 = 0.80-0.99$ ). The calculated  $k_2$  differed greatly among the BCPs within the  
464 group of herbal BCPs and the soot group, but was very close between the two woody  
465 BCPs. For a given BCPs, the  $k_2$  at a lower RH level was significantly larger than that  
466 at a higher RH level. Similar results were reported in previous studies on sorption  
467 kinetics of water vapor to activated carbon (Ohba and Kaneko, 2011; Ribeiro et al.,  
468 2008). Under low humidity conditions, sorption of water vapor mainly occurs at the  
469 active, high-energy binding sites, and the sorption kinetics is fast; alternatively, under  
470 high humidity conditions, sorption is governed by the slow pore-filling/condensation  
471 process of water molecules within the pores of activated carbon via formation of

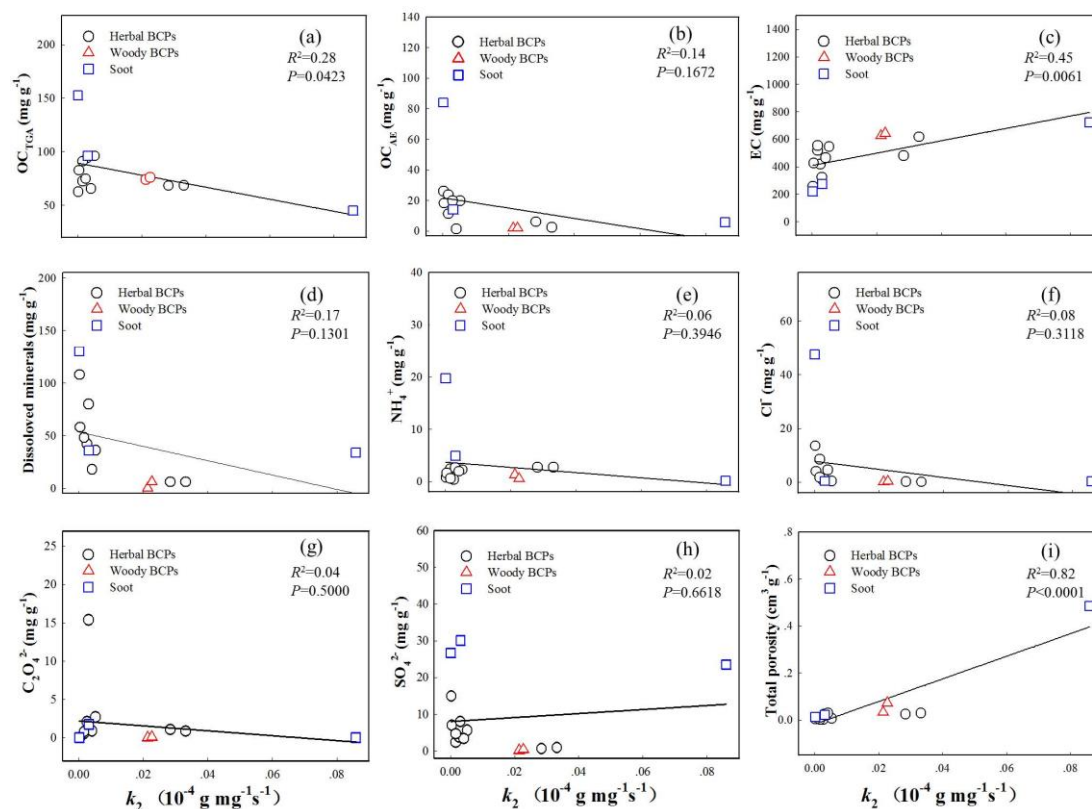
472 water clusters around the water molecules already sorbed at the active sites (Nguyen  
 473 and Bhatia, 2011; Rosas et al., 2008). Due to the small molecular size ( $0.0958 \times 0.151$   
 474 nm, ChemDraw 3D), water molecules could well penetrate into the micropores of  
 475 **BCPs** and form water clusters via intermolecular hydrogen bonding. The sorbing  
 476 ability order of the different types of **BCPs** varied depending on the examined RH. At  
 477 33% RH, the  $k_2$  roughly followed a decreasing order of soot ( $0.5\text{--}5.25 \times 10^{-5} \text{ g}$   
 478  $\text{mg}^{-1}\text{s}^{-1}$ ) > woody **BCPs** ( $1.57\text{--}1.90 \times 10^{-5} \text{ g mg}^{-1}\text{s}^{-1}$ ) > herbal **BCPs** ( $0.34\text{--}2.07 \times 10^{-5}$   
 479  $\text{g mg}^{-1}\text{s}^{-1}$ ); however, no clear trend was shown for high humidity conditions (e.g., RH  
 480 = 94%), mainly resulting from the larger variances within the **group of herbal BCPs**  
 481 and soot group.



482  
 483 Figure 4. Sorption kinetics of water vapor plotted as water uptake ( $\text{mg g}^{-1}$ ) vs. time (h)  
 484 at 94% relative humidity. (a) Subgroup 1 of herbal **BCPs**. (b) Subgroup 2 of herbal  
 485 **BCPs**. (c) Woody **BCPs**. (d) Soot. **Error bars represent standard variations from**

486 duplicate samples.

487 Like for the equilibrium water uptake, the relationships were built between the  $k_2$   
488 and the contents of  $OC_{TGA}$ ,  $OC_{AE}$ , EC, dissolved minerals, major ionic species ( $NH_4^+$ ,  
489  $Cl^-$ ,  $C_2O_4^{2-}$  and  $SO_4^{2-}$ ), and total porosity, respectively at 94% RH (Figure 5). The  
490 regression relationships at 33% RH were presented in Figure S11. The regression  
491 accuracy ( $R^2$  and  $P$ ) values at 33%, 47%, and 94% RH are summarized in Table S11.  
492 At 94% RH, a strong positive correlation was observed between the  $k_2$  and the total  
493 porosity ( $R^2 = 0.82$ ,  $P < 0.0001$ ), likely resulting from the pore-filling/condensation  
494 mechanism. A similar mechanism has been previously proposed to account for the  
495 positive correlation observed between the water vapor sorption kinetics and the  
496 porosity of activated carbon under high humidity conditions (Nakamura et al., 2010;  
497 Velasco et al., 2016). Likewise, a positive correlation ( $R^2 = 0.45$ ,  $P = 0.0061$ ) was  
498 observed between the  $k_2$  and the EC content, which could be ascribed to the formation  
499 of rigid pore structures dominantly by graphitized carbons (EC) (Han et al., 2014).  
500 The correlation between  $k_2$  and total porosity observed at 94% RH disappeared under  
501 low and medium humidity conditions. At 33% RH, relatively good positive  
502 correlations were observed with the contents of  $OC_{TGA}$  ( $R^2 = 0.47$ ,  $P = 0.0046$ ),  $OC_{AE}$   
503 ( $R^2 = 0.44$ ,  $P = 0.007$ ),  $NH_4^+$  ( $R^2 = 0.77$ ,  $P < 0.0001$ ), and  $Cl^-$  ( $R^2 = 0.60$ ,  $P =$   
504  $0.0007$ ), but not with  $SO_4^{2-}$  ( $R^2 = 0.11$ ,  $P = 0.2286$ ) or dissolved minerals ( $R^2 = 0.08$ ,  
505  $P = 0.31$ ). The positive correlations with these constituents were not shown under  
506 medium and high humidity conditions. Thus, the constituents of OC and  $NH_4^+$ - and  
507  $Cl^-$ -salts likely provided the primary high affinity, active sites for sorption of water  
508 vapor under low humidity conditions.



509

510 Figure 5. Relationships between pseudo-second water uptake rate constant ( $k_2$ ) (g  
 511  $\text{mg}^{-1}\text{s}^{-1}$ ) vs. compositional and pore property parameters for the **group of BCPs** at 94%  
 512 relative humidity. (a) TGA-measured organic carbon ( $\text{OC}_{\text{TGA}}$ ). (b) Alkali-extracted  
 513 organic carbon ( $\text{OC}_{\text{AE}}$ ). (c) Elemental carbon (EC). (d) Dissolved minerals. (e)  
 514 Ammonium ( $\text{NH}_4^+$ ). (f) Chloride ( $\text{Cl}^-$ ). (g) Oxalate ( $\text{C}_2\text{O}_4^{2-}$ ). (h) Sulfate ( $\text{SO}_4^{2-}$ ). (i)  
 515 Total porosity.

#### 516 4. Conclusion

517 The hygroscopic properties of 15 different **BCPs** (herbal, woody, and soot) were  
 518 systematically investigated using gravimetric method and DRIFTS. The mechanisms  
 519 and factors controlling the equilibrium and kinetic water uptake differed among the  
 520 types of **BCPs** and depended heavily on the humidity conditions. Linear correlation  
 521 analyses indicated that the equilibrium water uptake by the tested **group of BCPs**  
 522 positively correlated to the contents of OC ( $\text{OC}_{\text{TGA}}$  and  $\text{OC}_{\text{AE}}$ ), dissolved minerals,

523 and  $\text{NH}_4^+$  - and  $\text{Cl}^-$ -salts under high humidity conditions, and weakly to the contents of  
524 OC only under low humidity conditions. By contrast, negative correlations were  
525 observed between the equilibrium water uptake and the EC content. The low water  
526 uptake by the woody **BCPs** could be attributed to the very low contents of OC and  
527 dissolved minerals. Thus, the equilibrium water uptake by **BCPs** was mainly  
528 controlled by the hygroscopic constituents of OC and dissolved minerals/salts. The  
529 kinetic water uptake by the **BCPs** could be well described by the pseudo-second-order  
530 kinetic model. The calculated rate constant ( $k_2$ ) positively correlated to the contents  
531  $\text{OC}_{\text{TGA}}$ ,  $\text{OC}_{\text{AE}}$ , and  $\text{NH}_4^+$  - and  $\text{Cl}^-$ -salts under low humidity conditions, and to the total  
532 porosity only under high humidity conditions. The fast water uptake kinetics under  
533 low humidity conditions was attributed to the binding to high affinity, active sites (OC  
534 and salts), which could sorb water vapor fast but had limited contents. Alternatively,  
535 the slow water uptake kinetics under high humidity conditions was attributed to  
536 pore-filling/condensation of water molecules within the micro- and mesopores of  
537 **BCPs**. This study highlights that the hygroscopic properties of **BCPs** rely on  
538 compositional and structural properties of **BCPs** as well as humidity conditions.

539 **Author contributions.** DZ provided the original idea and prepared the paper with  
540 contributions from all co-authors. MW and YC designed and conducted the research,  
541 HF, XQ were involved in the development of the analysis methods. BL, ST reviewed  
542 the written document.

543 **Competing interests.** The authors declare that they have no conflict of interest.

544 **Acknowledgments.** This work was supported by the National Natural Science  
545 Foundation of China (Grants 21777002, 21920102002, and 41991331).

546 **Appendix A.**

547 Detailed characterization results of the different **BCPs** can be found in Tables

548 S1-S7. Table S8 lists accuracy ( $R^2$  and  $P$ ) values for regression on equilibrium water  
549 uptake against different variables. Tables S9-S10 present pseudo-first/second-order  
550 kinetic model fitting parameters. Table S11 lists accuracy ( $R^2$  and  $P$ ) values for  
551 regression on  $k_2$  against different variables. Figure S1-S4 displays spectroscopic  
552 characterization of different BCPs. Figure S5 displays sorption isotherms at selected  
553 humidity obtained by using saturated aqueous salt solutions. Figure S6 compares  
554 equilibrium water uptake measured by the two different gravimetric methods. Figure  
555 S7 displays relationships between equilibrium water uptake and different variables at  
556 23% RH. Figure S8 displays the Relationship between measured values of  
557 equilibrium water uptake at 94% relative humidity vs. predicted values obtained by  
558 binary factor regression based on contents of  $OC_{TGA}$  and dissolved minerals for the  
559 group of BCPs. Figure S9 compares equilibrium water uptake measured by DRIFTS  
560 and gravimetric method at high RH. Figure S10 displays sorption kinetics of water  
561 uptake at 33% RH. Figure S11 displays relationships between  $k_2$  and different  
562 variables at 33% RH.  
563

564 **References**

- 565 Adapa, S., Swamy, D. R., Kancharla, S., Pradhan, S., and Malani, A.: Role of mono-  
566 and divalent surface cations on the structure and adsorption behavior of water on  
567 mica surface, *Langmuir*, 34 (48), 2018.
- 568 Andreae, M. O., and Gelencser, A.: Black carbon or brown carbon? The nature of  
569 light-absorbing carbonaceous aerosols, *Atmos. Chem. Phys.*, 6, 3131–3148, 2006.
- 570 Archanjo, B. S., Araujo, J. R., Silva, A. M., Capaz, R. B., Falcao, N. P. S., Jorio, A.,  
571 and Achete, C. A.: Chemical analysis and molecular models for  
572 calcium-oxygen-carbon interactions in black carbon found in fertile Amazonian  
573 anthrosoils, *Environ. Sci. Technol.*, 48, 7445–7452, 2014.
- 574 Bond, T. C., Doherty, S. J., Fahey, D. W., Forster, P. M., Berntsen, T., DeAngelo, B. J.,  
575 Flanner, M. G., Ghan, S., Kärcher, B., Koch, D., Kinne, S., Kondo, Y., Quinn, P. K.,  
576 Sarofim, M. C., Schultz, M. G., Schulz, M., Venkataraman, C., Zhang, H., Zhang,  
577 S., Bellouin, N., Guttikunda, S. K., Hopke, P. K., Jacobson, M. Z., Kaiser, J. W.,  
578 Klimont, Z., Lohmann, U., Schwarz, J. P., Shindell, D., Storelvmo, T., Warren, S. G.,  
579 and Zender, C. S.: Bounding the role of black carbon in the climate system: A  
580 scientific assessment, *J. Geophys. Res. Atmos.*, 118, 5380–5552, 2013.
- 581 Buchholz, A., and Mentel, T. F.: Hygroscopic growth of oxalic acid and its ammonium,  
582 sodium and potassium salts, *Geophys. Res. Abs.*, 10, EGU2008-A-03795.
- 583 Cancado, L. G., Takai, K., Enoki, T., Endo, M., Kim, Y. A., and Mizusaki, H.: General  
584 equation for the determination of the crystallite size  $L_a$  of nanographite by Raman  
585 spectroscopy, *Appl. Phys. Lett.*, 88 (16), 2006.
- 586 Carrico, C. M., Petters, M. D., Kreidenweis, S. M., Sullivan, A. P., McMeeking, G. R.,  
587 Levin, E. J. T., Engling, G., Malm, W. C., and Collett Jr. J. L.: Water uptake and  
588 chemical composition of fresh aerosols generated in open burning of biomass,

589 Atmos. Chem. Phys., 10, 5165–5178, 2010.

590 Day, D. E., Hand, J. L., Carrico, C. M., Engling, G., and Malm, W. C.: Humidification  
591 factors from laboratory studies of fresh smoke from biomass fuels, *J. Geophys. Res.*,  
592 111, D22202, 2006.

593 Fletcher, A. J., Uygur, Y., and Mark Thomas, K.: Role of surface functional groups in  
594 the adsorption kinetics of water vapor on microporous activated carbons, *J. Phys.*  
595 *Chem. C.*, 111, 8349–8359, 2007.

596 Freney, E. J., Martin, S. T., and Buseck, P. R.: Deliquescence measurements of  
597 potassium salts, American Geophysical Union, Fall Meeting, 2007.

598 Ghorai, S., Laskin, A., and Tivanski, A. V.: Spectroscopic evidence of keto-enol  
599 tautomerism in deliquesced malonic acid particles, *J. Phys. Chem. A.*, 115,  
600 4373–4380, 2011.

601 Gu, W., Li, Y., Zhu, J., Jia, X., Lin, Q., Zhang, G., Ding, X., Song, W., Bi, X., Wang,  
602 X., and Tang, M.: Investigation of water adsorption and hygroscopicity of  
603 atmospherically relevant particles using a commercial vapor sorption analyzer,  
604 *Atmos. Meas. Tech.*, 10, 3821–3832, 2017.

605 Gustafsson, R. J., Orlov, A., Badger, C. L., Griffiths, P. T., Cox, R. A., and Lambert, R.  
606 M.: A comprehensive evaluation of water uptake on atmospherically relevant  
607 mineral surfaces: DRIFT spectroscopy, thermogravimetric analysis and aerosol  
608 growth measurements, *Atmos. Chem. Phys.*, 5, 3415–3421, 2005.

609 Haddrell, A. E., Davies, J. F., and Reid, J. P.: Dynamics of particle size on inhalation  
610 of environmental aerosol and impact on deposition fraction, *Environ. Sci. Technol.*,  
611 49, 14512–14521, 2015.

612 Han, C., Liu, Y., and He, H.: Role of organic carbon in heterogeneous reaction of NO<sub>2</sub>  
613 with soot, *Environ. Sci. Technol.*, 47, 3174–3181, 2013.

614 Han, L. F., Sun, K., Jin, J., Wei, X., Xia, X. H., Wu, F. C., Gao, B., and Xing, B. S.:  
615 Role of structure and microporosity in phenanthrene sorption by natural and  
616 engineered organic matter, *Environ. Sci. Technol.*, 48, 11227–11234, 2014.

617 Jing, B., Peng, C., Wang, Y., Liu, Q., Tong, S., Zhang, Y., and Ge, M.: Hygroscopic  
618 properties of potassium chloride and its internal mixtures with organic compounds  
619 relevant to biomass burning aerosol particles, *Sci. Rep.*, 2, 43573, 2017.

620 Keiluweit, M., Nico, P. S., Johnson, M. G., Kleber, M.: Dynamic molecular structure  
621 of plant biomass-derived black carbon (biochar), *Environ. Sci. Technol.*, 44 (4),  
622 1247–1253, 2010.

623 Lewis, K. A., Arnott, W. P., Moosmuller, H., Chakrabarty, R. K., Carrico, C. M. ,  
624 Kreidenweis, S. M., Day, D. E., Malm, W. C., Laskin, A., Jimenez, J. L., Ulbrich, I.  
625 M., Huffman, J. A., Onasch, T. B., Trimborn, A., Liu, L., and Mishchenko, M. I.:  
626 Reduction in biomass burning aerosol light absorption upon humidification: roles  
627 of inorganically-induced hygroscopicity, particle collapse, and photoacoustic heat  
628 and mass transfer, *Atmos. Chem. Phys.*, 9, 8949–8966, 2009.

629 Li, J., Posfai, M., Hobbs, P. V., and Buseck, P. R.: Individual aerosol particles from  
630 biomass burning in southern Africa: 2. Compositions and aging of inorganic  
631 particles, *J. Geophys. Res.*, 108, 8484, 2003.

632 Lian, F., and Xing, B.: Black carbon (biochar) in water/soil environments: Molecular  
633 structure, sorption, stability, and potential risk, *Environ. Sci. Technol.*, 51,  
634 13517–13532, 2017.

635 Liu, P., Song, M., Zhao, T., Gunthe, S. S., Ham, S., He, Y., Qin, Y. M., Gong, Z.,  
636 Amorim, J. C., Bertram, A. K., and Martin, S. T.: Resolving the mechanisms of  
637 hygroscopic growth and cloud condensation nuclei activity for organic particulate  
638 matter, *Nat. Commun.*, 9, 4076, 2018.

639 Ma, Q., He, H., Liu, Y.: In situ DRIFTS study of hygroscopic behavior of mineral  
640 aerosol, *J. Environ. Sci.*, 22(4), 555–560, 2010.

641 Matthews, H. D., Gillett, N. P., Stott, P. A., and Zickfeld, K.: The proportionality of  
642 global warming to cumulative carbon emissions, *Nature*, 459, 829–832, 2009.

643 Nakamura, M., Ohba, T., Branton, P., Kanoh, H., and Kaneko, K.: Equilibrium-time  
644 and pore width dependent hysteresis of water adsorption isotherm on hydrophobic  
645 microporous carbons, *Carbon*, 48, 2549–2553, 2010.

646 Nguyen, T. X., and Bhatia, S. K.: How water adsorbs in hydrophobic nanospaces, *J.*  
647 *Phys. Chem. C*, 115, 16606–16612, 2011.

648 Nienow, A. M., Roberts, J. T.: Heterogeneous chemistry of carbon aerosols, *Rev. Phys.*  
649 *Chem.*, 57, 105–128, 2006.

650 Ohba, T., and Kaneko, K.: Kinetically forbidden transformations of water molecular  
651 assemblies in hydrophobic micropores, *Langmuir*, 27, 7609–7613, 2011.

652 Petters, S. S., Pagonis, D., Clafin, M. S., Levin, E. J. T., Petters, M. D., Ziemann, P. J.,  
653 and Kreidenweis, S. M.: Hygroscopicity of organic compounds as a function of  
654 carbon chain length and carboxyl, hydroperoxy, and carbonyl functional groups, *J.*  
655 *Phys. Chem. A*, 121 (27), 5164–5174, 2017.

656 Pimenta, M. A., Dresselhaus, G., Dresselhaus, M. S., Cancado, L. G., Jorio, A., and  
657 Saito, R.: Studying disorder in graphite-based systems by Raman spectroscopy,  
658 *Phys. Chem. Chem. Phys.*, 9, 1276–1291, 2007.

659 Posfai, M., Simonic, R., Li, J., Hobbs, P. V., and Buseck, P. R.: Individual aerosol  
660 particles from biomass burning from southern Africa: 1. Compositions and size  
661 distributions of carbonaceous particles, *J. Geophys. Res.*, 108, 8483, 2003.

662 Powelson, M. H., Espelien, B. M., Hawkins, L. N., Galloway, M. M., and De Haan, D.  
663 O.: Brown carbon formation by aqueous-phase carbonyl compound reactions with

664 amines and ammonium sulfate, *Environ. Sci. Technol.*, 48, 985–993, 2014.

665 Preturlan, J. G. D., Vieille, L., Quiligotti, S., and Favergeon, L.: Comprehensive  
666 thermodynamic study of the calcium sulfate–water vapor system. Part 1:  
667 experimental measurements and phase equilibria, *Ind. Eng. Chem. Res.*, 58, 22,  
668 9596–9606, 2019.

669 Qiu, C., Khalizov, A. F., and Zhang, R.: Soot aging from OH-Initiated oxidation of  
670 toluene, *Environ. Sci. Technol.*, 46, 9464–9472, 2012.

671 Reid, J. S., Koppmann, R., Eck, T. F., and Eleuterio, D. P.: A review of biomass  
672 burning emissions part II: intensive physical properties of biomass burning particles,  
673 *Atmos. Chem. Phys.*, 5, 799–825, 2005.

674 Ribeiro, A. M., Sauer, T. P., Grande, C. A., Moreira, R. F. P. M., Loureiro, J. M., and  
675 Rodrigues, A. E.: Adsorption equilibrium and kinetics of water vapor on different  
676 adsorbents, *Ind. Eng. Chem. Res.*, 47, 18, 7019–7026, 2008.

677 Rosas, J. M., Bedia, J., Miraso, J. R., and Cordero, T.: Preparation of hemp-derived  
678 activated carbon monoliths, adsorption of water vapor, *Ind. Eng. Chem. Res.*, 47, 4,  
679 1288–1296, 2008.

680 Schwarz, J. P., Spackman, J. R., Fahey, D. W., Gao, R. S., Lohmann, U., Stier, P.,  
681 Watts, L. A., Thomson, D. S., Lack, D. A., Pfister, L., Mahoney, M. J.,  
682 Baumgardner, D., Wilson, J. C., and Reeves, J. M.: Coatings and their enhancement  
683 of black carbon light absorption in the tropical atmosphere, *J. Geophys. Res.*, 113,  
684 D03203, 2008.

685 Seisel, S., Pashkova, A., Lian, Y., and Zellner, R.: Water uptake on mineral dust and  
686 soot: a fundamental view of the hydrophilicity of atmospheric particles, *Faraday*  
687 *Discuss.*, 130, 437–451, 2005.

688 Sjogren, S., Gysel, M., Weingartner, E., Baltensperger, U., Cubison, M. J., Coe, H.,

689 Zardini, A. A., Marcolli, C., Krieger, U. K., and Peter, T.: Hygroscopic growth and  
690 water uptake kinetics of two-phase aerosol particles consisting of ammonium  
691 sulfate, adipic and humic acid mixtures, *Aerosol Science*, 38, 157–171, 2007.

692 Song, J., Peng, P., and Huang, W.: Black carbon and kerogen in soils and sediments. 1.  
693 Quantification and characterization, *Environ. Sci. Technol.*, 36, 3960–3967, 2002.

694 Song, W., and Boily, J. F.: Water vapor adsorption on goethite, *Environ. Sci. Technol.*,  
695 47, 7171–7177, 2013.

696 Stanislav, V., Vassilev, D. B., Andersen, L. K., and Vassileva, C. G.: An overview of  
697 the composition and application of biomass ash. Part 1. Phase-mineral and chemical  
698 composition and classification, *Fuel*, 105, 40–76, 2013.

699 Stemmler, K., Vlasenko, A., Guimbaud, C., and Ammann, M.: The effect of fatty acid  
700 surfactants on the uptake of nitric acid to deliquesced NaCl aerosol, *Atmos. Chem.*  
701 *Phys.*, 2008, 8 (17), 5127–5141, 2008.

702 Suda, S. R., Petters, M. D., Yeh, G. K. Strollo, C., Matsunaga, A., Faulhaber, A.,  
703 Ziemann, P. J., Prenni, A. J., Carrico, C. M., Sullivan, R. C., and Kreidenweis, S.  
704 M.: Influence of functional groups on organic aerosol cloud condensation nucleus  
705 activity, *Environ. Sci. Technol.*, 48, 10182–10190, 2014.

706 Velasco, L. F., Remy Guillet, N. R., Dobos, G., Thommes, M., and Lodewyckx, P.:  
707 Towards a better understanding of water adsorption hysteresis in activated carbons  
708 by scanning isotherms, *Carbon*, 96, 753–758, 2016.

709 Wei, S., Zhu, M., Fan, X., Song, J., Peng, P., Li, K., Jia, W., and Song, H.: Influence  
710 of pyrolysis temperature and feedstock on carbon fractions of biochar produced  
711 from pyrolysis of rice straw, pine wood, pig manure and sewage sludge,  
712 *Chemosphere*, 218, 624–631, 2019.

713 Xiao, J., Liu, Z., Kim, K., Chen, Y., Yan, J., Li, Z., and Wang, W.: S/O-Functionalities

714 on modified carbon materials governing adsorption of water vapor, *J. Phys. Chem.*  
715 *C.*, 117, 23057–23065, 2013.

716 Xiao, X., Chen, B., Chen, Z., Zhu, L., and Schnoor, J. L.: Insight into multiple and  
717 multilevel structures of biochars and their potential environmental applications: A  
718 critical review, *Environ. Sci. Technol.*, 52(9), 5027–5047, 2018.

719 Yuan, J. F., Huang, X. F., Cao, L. M., Cui, J., Zhu, Q., Huang, C. N., Lan, Z. J., and  
720 He, L.Y.: Light absorption of brown carbon aerosol in the PRD region of China,  
721 *Atmos. Chem. Phys. Discuss.*, 15, 28453–28482, 2015.

722 Yuan, W., Li, X., Pan, Z., Connell, L. D., Li, S., and He, J.: Experimental  
723 investigation of interactions between water and a lower silurian chinese shale,  
724 *Energy Fuels*, 28, 4925–4933, 2014.

725 Zhang, R., Khalizov, A., Wang, L., Hu. M., and Xu, W.: Nucleation and growth of  
726 nanoparticles in the atmosphere, *Chem. Rev.*, 112, 3, 1957–2011, 2012.

727 Zuend, A., Marcolli, C., Booth, A. M., Lienhard, D. M., Soonsin, V., Krieger, U. K.,  
728 Topping, D. O., McFiggans, G., Peter, T., and Seinfeld, J. H.: New and extended  
729 parameterization of the thermodynamic model AIOMFAC: Calculation of activity  
730 coefficients for organic-inorganic mixtures containing carboxyl, hydroxyl, carbonyl,  
731 ether, ester, alkenyl, alkyl, and aromatic functional groups, *Atmos. Chem. Phys.*, 11,  
732 9155–9206, 2011.